

Engineering multipartite entanglement in doubly pumped parametric down-conversion processes

Alessandra Gatti^{1,2}, Enrico Brambilla² and Ottavia Jedrkiewicz^{3,2}

¹ *Istituto di Fotonica e Nanotecnologie (IFN-CNR), Piazza Leonardo Da Vinci 32, Milano, Italy;* ² *Dipartimento di Scienza e Alta Tecnologia dell' Università dell'Insubria, Via Valleggio 11, Como, Italy;* ³ *Istituto di Fotonica e Nanotecnologie (IFN-CNR), Via Valleggio 11, Como, Italy* *

We investigate the quantum state generated by optical parametric down-conversion in a $\chi^{(2)}$ medium driven by two noncollinear light modes. The analysis shows the emergence of multipartite, namely 3- or 4-partite, entangled states in a subset of the spatio-temporal modes generated by the process. These appear as bright spots against the background fluorescence, providing an interesting analogy with the phenomenology recently observed in two-dimensional nonlinear photonic crystals. We study two realistic setups: i) Non-critical phase-matching in a periodically poled Lithium Tantalate slab, characterized by a 3-mode entangled state. ii) A type I setup in a Beta-Barium Borate crystal, where the spatial walk-off between the two pumps can be exploited to make a transition to a quadripartite entangled state. In both cases we show that the properties of the state can be controlled by modulating the relative intensity of two pump waves, making the device a versatile tool for quantum state engineering.

PACS numbers: 42.65.Lm, 42.50.Ar, 42.50.Dv

arXiv:2007.12014v3 [quant-ph] 19 Nov 2020

* Alessandra.Gatti@ifn.cnr.it

INTRODUCTION

Multipartite entanglement, where quantum entanglement is shared by more than two physical systems, is a key resource, both from fundamental [1] and applicative viewpoints. In optics, an efficient tool able to prepare and engineer multiparty entangled states of light would be an asset for several quantum technologies: among them, measurement-based quantum computation [2, 3], which require to generate multipartite entangled cluster states [4, 5] in a controlled and re-configurable way, and quantum metrological schemes of distributed quantum sensing [6]. Nevertheless, the most efficient sources of quantum optical states are nonlinear processes, as four-wave mixing and parametric down-conversion (PDC), that generate photons in pairs, which naturally leads to bipartite Einstein-Podolsky-Rosen (EPR) entanglement and to squeezed states. Then, in the continuous variable regime, a well-established scheme for producing multipartite entanglement requires an external manipulation of such squeezed states by mixing them in a network of passive optical elements (see e.g. [7–9]). External manipulations of the squeezed or EPR states generated by nonlinear optical process are also necessary for other fundamental tasks of quantum information, e.g. in order to introduce non-Gaussianity and to enable entanglement distillation, as in protocols of photon-subtraction where a small fraction of the light is redirected towards a photon counting detector, and the remaining state is conditioned upon detection of photons (see e.g. [10, 11]).

In this work we follow a different approach, aiming at engineering the nonlinear process which is source of squeezing itself by acting on the spatial degrees of freedom of the pump beam driving the process. Ideally, the goal is directly producing the desired state and/or implementing some operations of interest for quantum technologies. In a sense, we propose to invert the order of the above mentioned steps, by transferring the linear manipulations from the squeezed modes generated by the process to the spatial modes of the classical laser pump beam. This approach has a number of advantages: first, avoiding as much as possible manipulations of the fragile quantum states, operating instead on the more robust classical pump; second, the possibility of engineering the state by modulating the properties of the pump; finally, as we shall see, the fact that multipartite entanglement is produced among spatial modes of the same beam, which are already separated. In this proposal we consider using two pump beams slightly tilted in the transverse direction to drive parametric down-conversion in a $\chi^{(2)}$ medium.

The idea is not completely new: an ideal scheme was explored in [12], where a tripartite entanglement was theoretically predicted. The use of a spatially structured pump with a TEM_{01} modal profile, to produce peculiar spatial correlation between twin photons was also explored in [13]. More recently, a scheme for engineering the quantum and classical properties of parametric generation by dual pumping a 2D nonlinear photonic crystal was proposed by some of us [14, 15]. Several four-wave mixing schemes, exploiting the $\chi^{(3)}$ nonlinearity, with dual spatial pump modes have been recently studied and experimentally realized [16–18].

The problem with down-conversion, intrinsically more efficient than four-wave mixing, is that both the phase matching and the effective nonlinearity depend on the direction of propagation of each pump beam, making the scheme more complex. Therefore, a large part of this work will be devoted to the characterization of the simultaneous phase-matching of the concurrent nonlinear processes driven by the two pumps. Two concrete setups will be explored:

The first scheme considers a type 0 process in a periodically poled Lithium Tantalate (PPLT) slab, where the two pumps are tilted in the plane perpendicular to the optical axis of the crystal, so that neither the phase matching nor the nonlinearity depend on the direction of propagation of the modes. We show that this is the ideal framework to realize the proposal in [12], and that a 3-mode entanglement is realized in specific subsets of spatio-temporal modes, which appear as bright hot-spots against the less intense background due to standard 2-mode fluorescence. With respect to [12], we analyse the more general case of arbitrary pump amplitudes, and, as schematically shown by Fig.1, we find that the tripartite entangled state thereby realized is formally equivalent to dividing one of the parties of a bipartite EPR state on a beam-splitter whose reflection and transmission coefficients are in the same ratio as two pump intensities. This result may be relevant for photon-subtraction protocols, because it shows that the doubly-pumped scheme implements an arbitrary beam-splitter, without the need of external alignments potentially detrimental for the quantum state.

The second scheme considers a type I process in a standard Beta-Barium-Borate (BBO) crystal, where the pumps are tilted in a direction that is not perpendicular to the optical axis. The analysis here is strictly connected to a parallel experimental work [19]. In this configuration, we show that the strong birefringence of the BBO crystal, responsible for spatial walk-off effects, can be exploited to identify peculiar directions of propagation of the two pumps inside the crystal, such that two triplets of hot-spots, originally uncoupled, merge into quadruplets of entangled modes, with a sudden enhancement of the intensity of hot-spots [19]. These *resonances*, as we shall call them, will be interpreted in terms of a superposition of the mean flux of the pump energy (the Poynting vector of the carrier wave) with the direction of propagation of one of the pump modes. From a quantum viewpoint, we will show that the quadripartite entangled state thereby generated can be formally described as the interference of a *pair* of independent EPR states, as schematically described by Fig.2. Remarkably, the squeezing and the mixing parameters turn out to be controlled by the relative intensity of the pumps, giving access to a potential control over the state.

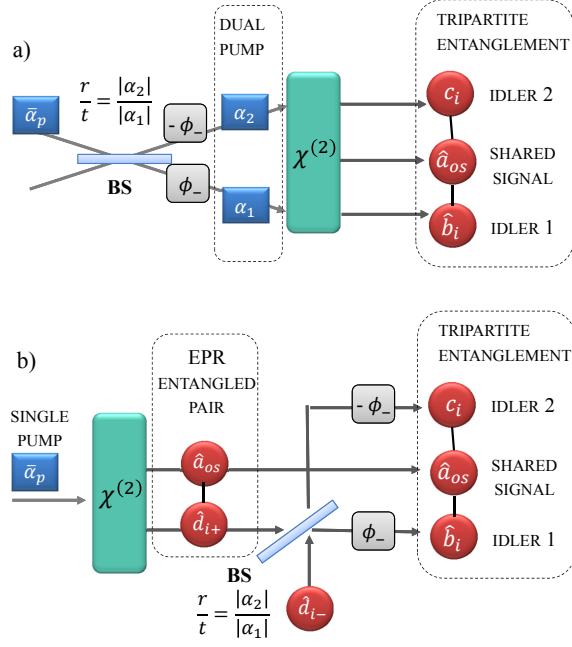


FIG. 1. a) Schematic of the dual pump source, where two non-collinear modes of amplitudes α_1 and α_2 pump a $\chi^{(2)}$ medium, and generate a tripartite entangled state in specific sets of spatio-temporal modes (Sec.II B). The two pumps can be seen as deriving from a single pump $\bar{\alpha}_p = \sqrt{|\alpha_1|^2 + |\alpha_2|^2}$. We will show that the source is formally equivalent to the scheme b), in which the medium is pumped by a single beam of amplitude $\bar{\alpha}_p$, and one of the two parties of the EPR state thereby generated is mixed with an arbitrary input mode \hat{d}_{i-} on a beam-splitter with reflection and transmission coefficients $\frac{r}{t} = \frac{|\alpha_2|}{|\alpha_1|}$. ϕ_- are local phase shift by half of the pump phase difference.

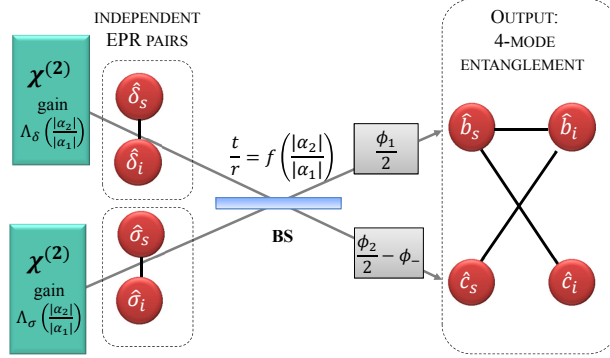


FIG. 2. Decomposition of the 4-mode entangled state generated by a doubly pumped BBO in the *resonance* conditions demonstrated in Sec.III. This is equivalent to a pair of independent EPR states mixed on a beam-splitter BS and followed by phase rotations (gray boxes). The squeeze parameters $\Lambda_\sigma, \Lambda_\delta$ of the EPR states, and the BS transmission and reflection coefficients are controlled by the intensity ratio of the two pump modes (see Eqs.(34) and (35)). The description holds for specific quadruplets of spatio-temporal modes which will be characterized in Sec. III A.

On a different perspective, our work highlights a striking analogy with the phenomenology recently observed in a 2-dimensional nonlinear photonic crystal (NPC) [20, 21], including not only the emergence of hot-spots in correspondence of triplets of entangled modes, but also the existence of the resonance that leads to a 4-mode entangled state, which in the case of the NPC was named *Golden Ratio Entanglement*. These two apparently disparate systems have the common feature that two concurrent nonlinear processes coexist in the same medium, as will be discussed in Sec.IA

The paper is organized as follows: Section I introduces the general theoretical framework and discusses the analogy between the doubly pumped scheme and parametric generation in nonlinear photonic crystals. Sec.II analyses the PPLT case and the tripartite entanglement associated with it, with a blend of analytical calculations, performed in the parametric limit, and numerical simulations. Sec.III analyses the BBO case, the transition to resonance and the

4-mode entanglement. Numerical and experimental data for this part are presented in the related work [19].

I. GENERAL FRAMEWORK

This section introduces the general theoretical framework, formulated in terms of 3D+1 propagation equations inside the nonlinear $\chi^{(2)}$ material for the quantum field operators associated with the interacting light fields.

Our work focuses on a degenerate type 0 or type I process, in which the down-converted light is described by a single field envelope centered around half of the pump frequency. Thus, we consider the two slowly varying field operators associated with the high-frequency pump and the low-frequency down-converted signal, which in the Fourier domain read: $\hat{A}_j(\vec{q}, \Omega, z) = \int \frac{d^2\vec{r}}{2\pi} \int \frac{dt}{\sqrt{2\pi}} e^{i(\omega_j + \Omega)t} e^{-i[k_{jz}(\vec{q}, \Omega)z + \vec{q} \cdot \vec{r}]} \hat{E}_j(\vec{r}, z, t)$, ($j = p, s$) (see [22, 23] for details), where: z is the mean direction of propagation of the fields, assumed to be paraxial waves; Ω_j is the frequency shift from the carriers ω_p and $\omega_s = \frac{\omega_p}{2}$; $\vec{q} = q_x \vec{e}_x + q_y \vec{e}_y$ is the transverse component of the wave-vector; $k_{jz}(\vec{q}, \Omega) = \sqrt{k_j^2(\vec{q}, \Omega) - q^2}$ is its z -component, where $k_j(\vec{q}, \Omega) = n_j(\vec{q}, \omega_j + \Omega) \frac{\omega_j + \Omega}{c}$ is the wave-number, $n_j(\vec{q}, \omega)$ being the index of refraction of the j -th wave. For the extraordinary wave, the index depends both on the frequency and on the direction of propagation, implicitly identified by the transverse wave-vector component \vec{q} . Finally, $\hat{E}_j(\vec{r}, z, t)$ is the full field operator in the direct space, such that $\hat{E}_j^\dagger \hat{E}_j$ has the dimensions of a photon number per unit area and unit time. By using the shorthand notation $\vec{w} \equiv (\vec{q}, \Omega) \in \mathbb{R}^3$, the coupled propagation equations have the form:

$$\frac{\partial}{\partial z} \hat{A}_s(\vec{w}_s, z) = \int \frac{d^3\vec{w}_p}{(2\pi)^{\frac{3}{2}}} \chi(\vec{w}_p; \vec{w}_s) \hat{A}_p(\vec{w}_p, z) \hat{A}_s^\dagger(\vec{w}_p - \vec{w}_s, z) e^{-i\mathcal{D}(\vec{w}_s; \vec{w}_p)z} \quad (1a)$$

$$\frac{\partial}{\partial z} \hat{A}_p(\vec{w}_p, z) = -\frac{1}{2} \int \frac{d^3\vec{w}_s}{(2\pi)^{\frac{3}{2}}} \chi(\vec{w}_p; \vec{w}_s) \hat{A}_s(\vec{w}_s, z) \hat{A}_p(\vec{w}_p - \vec{w}_s, z) e^{i\mathcal{D}(\vec{w}_s; \vec{w}_p)z} \quad (1b)$$

The two equations describe all the possible down- and up-conversion processes between a pump photon in mode \vec{w}_p and a pair of signal and idler photons in modes \vec{w}_s and $\vec{w}_i = \vec{w}_p - \vec{w}_s$, satisfying the energy and transverse momentum conservation (for simplicity, we assumed that the crystal is infinite in the transverse directions). The conservation of longitudinal momentum is less stringent because of the finite longitudinal size of the medium, and is expressed by the phase-mismatch function

$$\mathcal{D}(\vec{w}_s; \vec{w}_p) = k_{sz}(\vec{w}_s) + k_{sz}(\vec{w}_p - \vec{w}_s) - k_{pz}(\vec{w}_p) + G_z \quad (2)$$

where we allow for the possibility of a longitudinal 1D poling of the material, such that the reciprocal vector of the nonlinear grating $G_z = \frac{2\pi}{\Lambda_{pol}}$ contributes to the momentum balance. For more generality, we also leave the possibility for the effective nonlinearity to depend on the direction of propagation of the three waves, through $\chi(\vec{w}_p, \vec{w}_s) \propto d_{eff}(\vec{w}_p, \vec{w}_s) \sqrt{\frac{\hbar\omega_p\omega_s^2}{8\epsilon_0 c^3 n_e(\omega_p) n_o^2(\omega_s)}}$. In standard configurations, where the pump is a weakly focused Gaussian beam propagating around a single direction, this dependence can be neglected. When the pump transverse profile is structured, in particular when it is formed by several waves propagating at different angles, the effective nonlinearity can significantly differ in each direction.

The nonlinear equations (1) have been numerically simulated, by means of fully 3D +1 simulations (see [24] and methods of [20]), which take into account a broad frequency bandwidth, typically on the order of 200-400 nm. The pump modes are modelled by two Gaussian pump pulses, of duration $\simeq 1$ ps and transverse waist $\simeq 400\mu\text{m}$, which propagate close to the z axis tilted one with respect to the other by few degrees.

A. Multiple pump waves, analogy with Nonlinear Photonic Crystals

Although numerical simulations can fully account for pump depletion effects, in the remaining of this work we shall largely exploit the undepleted pump limit. Thus we focus on Eq.(1a) only, with the pump field operator $\hat{A}_p(\vec{w}_p, z)$ replaced by the classical envelope $\mathcal{A}_p(\vec{w}_p)$ describing the profile of the injected pump. In particular, we consider the injection of multiple plane-wave modes, propagating at slightly different directions around the z -axis, i.e.

$$\mathcal{A}_p(\vec{q}, \Omega) = (2\pi)^{\frac{3}{2}} \delta(\Omega = 0) \sum_m \alpha_m \delta(\vec{q} - \vec{Q}_m) \quad (3)$$

Neglecting for simplicity in Eq (1a) the dependence of the effective nonlinearity on the propagation direction, we can then build a straightforward analogy with the process of parametric generation in 2D nonlinear photonic crystals

[25, 26]. In such materials, the nonlinear response of the medium is artificially modulated, typically via ferroelectric poling, according to a 2D periodic pattern, the pattern lying in a plane (x, z) perpendicular to the optical axis, including thus one transverse direction. The transverse modulation of the nonlinear response can be often reduced to $\chi(q_x) \rightarrow \sum_m \chi_m \delta(q_x - \vec{G}_m)$, where \vec{G}_m are the transverse components of the reciprocal vectors of the nonlinear lattice participating to quasi phase-matching [27]. For example, for a hexagonally poled crystal $\vec{G}_m = \pm G \vec{e}_x$ are the transverse components of the two fundamental reciprocal lattice vectors (see [15, 20, 21]). According to Eq.(1a), it is therefore equivalent to inject a single plane-wave pump into a photonic crystal equipped with several non-collinear reciprocal lattice vectors, or to inject several non-collinear pumps into a standard crystal (or into a 1D poled crystal). In a less formal way, the down-conversion process from an undepleted pump beam is ruled by the product of the medium nonlinear response and the pump profile: thus it is equivalent to structure the transverse profile of either one or the other. In the following of this work we shall indeed show that the behaviour of a nonlinear photonic crystal can be fully mimicked by injecting two non-collinear pumps, with the additional benefit that the dual pump scheme enables a reconfigurable control over the properties of the process, by modulating the pump amplitudes.

II. TYPE 0 PROCESS: TRIPARTITE ENTANGLEMENT

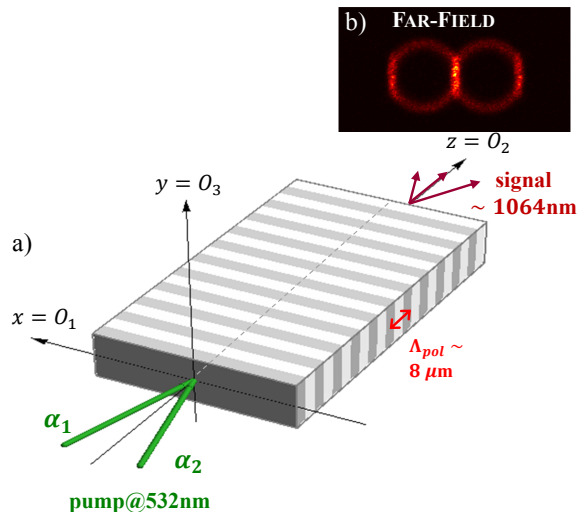


FIG. 3. a) Geometry of the scheme for the $e \rightarrow e, e$ process in a periodically poled LiTaO₃ slab. O_1, O_2, O_3 are the crystal principal axes. All the fields are polarized along the optical O_3 axis, and propagate at small angles with the O_2 axis. The pumps are slightly tilted along $x = O_1$. b) Far-field distribution of down-converted light from numerical simulations (see text). The plot shows a 20nm bandwidth around 1064nm.

This section studies the simplest configuration: a type O process where all the waves are extraordinarily polarized, pumped by two beams that propagate noncollinearly in the plane perpendicular to the optical axis.

For definiteness, we consider a periodically poled LiTaO₃ slab¹, with a poling period $\Lambda_{pol} \simeq 7.9 \mu\text{m}$, suitable to phase-match the type O interaction $\lambda_p = 532\text{nm} \rightarrow \lambda_s = \lambda_i = 1064\text{nm}$ at a temperature of $T \approx 75^\circ$. Fig.3 shows the geometry of the scheme: $O_3 \equiv y$ is the optical axis of the crystal; the crystalline $O_2 \equiv z$ axis represents the mean propagation direction of all waves; the two injected pump waves are slightly tilted in the $O_1 \equiv x$ direction, and thus propagate in the plane perpendicular to the optical axis. In these conditions, also known as *non-critical phase matching*, their wave numbers do not depend on the tilt angle, and, assuming a paraxial propagation, also the nonlinear coefficient does not depend to a good approximation on their propagation directions.

We approximate the pumps as classical plane-waves of complex amplitudes α_1 and α_2 , characterized by transverse

¹ The analysis can be straightforwardly extended to PPLN, we choose LiTaO₃ as an active material because of its very small birefringence

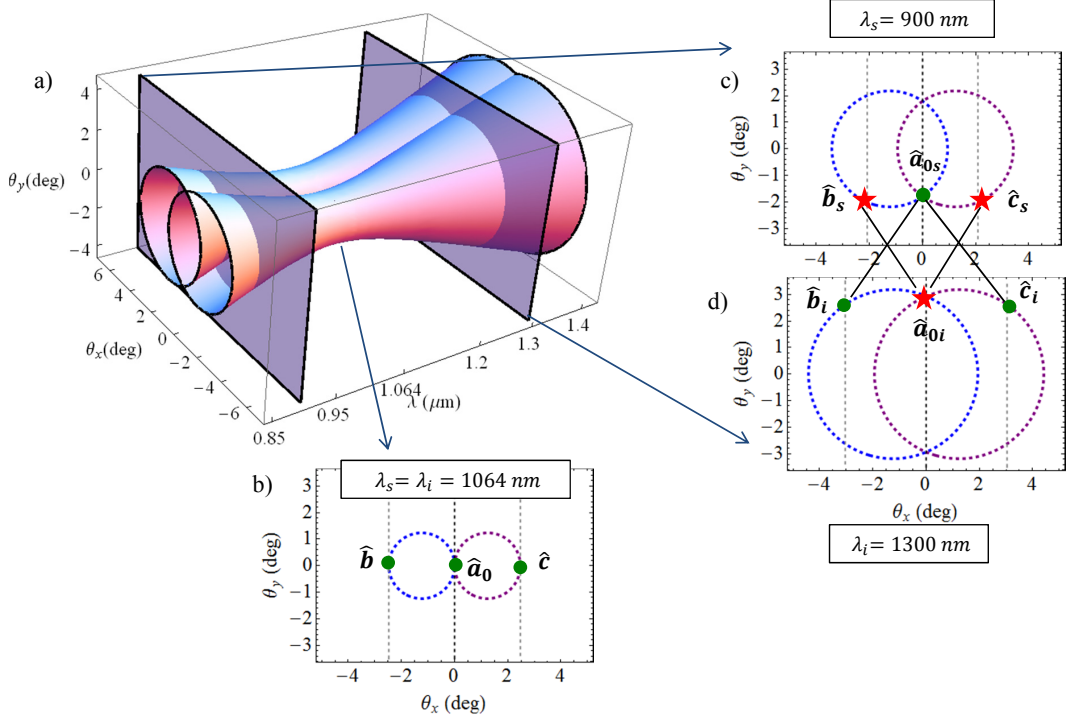


FIG. 4. PPLT doubly pumped at 532nm, by two pumps tilted at $\theta_{p1,p2} = \mp 1.2^\circ$ (internal angle). (a) Surfaces in the $(\lambda, \theta_x, \theta_y)$ space defining phase-matching for each pump mode [see Eq.(5)], calculated with the Sellmeier formulas in [28], for $T=75^\circ$ and $\Lambda_{pol} = 7.79\mu\text{m}$. (b) Section at $\lambda_s = \lambda_i = 1064\text{nm}$, showing the triplet of entangled modes. (c) and (d): Sections at two conjugate wavelengths $\lambda_s = 900\text{nm}$, $\lambda_i = 1300\text{nm}$, showing two independent triplets of modes (stars and dots).

wave vectors $\vec{Q}_1 = Q_1 \vec{e}_x$, $\vec{Q}_2 = Q_2 \vec{e}_x$, where $|Q_m| \ll \frac{2\pi}{\lambda_p}$. By substituting into Eq. (1a), we get:

$$\begin{aligned} \frac{\partial}{\partial z} \hat{A}_s(\vec{w}, z) = \chi \left[\alpha_1 \hat{A}_s^\dagger(\vec{Q}_1 - \vec{w}, z) e^{-i\mathcal{D}(\vec{w}; \vec{Q}_1)z} \right. \\ \left. + \alpha_2 \hat{A}_s^\dagger(\vec{Q}_2 - \vec{w}, z) e^{-i\mathcal{D}(\vec{w}; \vec{Q}_2)z} \right], \end{aligned} \quad (4)$$

where $\chi \simeq \chi(\vec{w}_{p1}; \vec{w}) = \chi(\vec{w}_{p2}; \vec{w})$ is the common value of the nonlinear coefficient. The r.h.s of Eq. (4) shows the contribution of the two processes originating from each pump. For the large majority of modes, only one of the two processes is phase-matched, giving rise to two noncollinear branches of down-converted modes (examples are shown in Fig. 4), corresponding to the standard conical emission around each pump taken separately. In the Fourier space (\vec{q}, Ω) photon pairs down-converted from each pump populate surfaces of equation

$$\begin{aligned} \Sigma_1 : \mathcal{D}(\vec{w}; \vec{Q}_1) = 0, \quad \text{pump 1} \\ \Sigma_2 : \mathcal{D}(\vec{w}; \vec{Q}_2) = 0 \quad \text{pump 2} \end{aligned} \quad (5)$$

A light mode \vec{w} belonging to the branch Σ_1 (Σ_2), but not to the intersection $\Sigma_1 \cap \Sigma_2$, hosts signal photons down-converted from pump 1 (2), whose twin idler photon is generated in a single coupled mode $\vec{Q}_1 - \vec{w}$ ($\vec{Q}_2 - \vec{w}$), giving rise to the standard two-mode coupling of PDC. Conversely, the modes lying at the geometrical intersection $\Sigma_1 \cap \Sigma_2$ are special, because here phase-matching is simultaneously realized for both pumps. Therefore, a photon appearing in one of these *shared* modes has been down-converted from either pump 1 or 2, indistinguishably. Its twin photon

appears in either one of *two coupled* modes, which evolve according to:

$$\begin{aligned} \frac{\partial}{\partial z} \hat{A}_s(\vec{Q}_1 - \vec{w}, z) &= \chi \left[\alpha_1 \hat{A}_s^\dagger(\vec{w}, z) e^{-i\mathcal{D}(\vec{w}; \vec{Q}_1)z} \right. \\ &\quad \left. + \alpha_2 \hat{A}_s^\dagger(\vec{Q}_2 - \vec{Q}_1 + \vec{w}, z) e^{-i\mathcal{D}(\vec{Q}_1 - \vec{w}; \vec{Q}_2)z} \right], \end{aligned} \quad (6)$$

$$\begin{aligned} \frac{\partial}{\partial z} \hat{A}_s(\vec{Q}_2 - \vec{w}, z) &= \chi \left[\alpha_2 \hat{A}_s^\dagger(\vec{w}, z) e^{-i\mathcal{D}(\vec{w}; \vec{Q}_2)z} \right. \\ &\quad \left. + \alpha_1 \hat{A}_s^\dagger(\vec{Q}_1 - \vec{Q}_2 + \vec{w}, z) e^{-i\mathcal{D}(\vec{Q}_2 - \vec{w}; \vec{Q}_1)z} \right], \end{aligned} \quad (7)$$

where we used the fact that $\mathcal{D}(\vec{Q}_m - \vec{w}; \vec{Q}_m) = \mathcal{D}(\vec{w}; \vec{Q}_m)$, ($m = 1, 2$), implicit in the definition (2) of the phase-mismatch function. In the present configuration, as shown in Sec.II B, if the shared mode condition

$$\mathcal{D}(\vec{w}_0; \vec{Q}_1) = \mathcal{D}(\vec{w}_0; \vec{Q}_2) \simeq 0 \quad (8)$$

is satisfied for a mode \vec{w}_0 , then the second of the two processes appearing at r.h.s of Eqs. (6) and (7) is not phase matched, that is, $\mathcal{D}(\vec{Q}_2 - \vec{w}_0; \vec{Q}_1)$ and $\mathcal{D}(\vec{Q}_1 - \vec{w}_0; \vec{Q}_2)$ are significantly different from zero. In other words, if the mode \vec{w}_0 is shared, then its two coupled modes cannot be themselves shared. This leads to the tripartite entangled state that will be described in the next section.

A. Tripartite entanglement

Let us concentrate on a specific triplet of modes whose coordinates \vec{w}_0 (shared mode) and $\vec{w}_{b,c} = \vec{Q}_{1,2} - \vec{w}_0$ (modes coupled to \vec{w}_0 via pump 1 and 2, respectively) are a solution of Eq.(8), as for example the modes shown by the dots in Fig.4c,d. Indicating by $\hat{a}_{0s} := \hat{A}_s(\vec{w}_0)$, $\hat{b}_i := \hat{A}_s(\vec{Q}_1 - \vec{w}_0)$, $\hat{c}_i := \hat{A}_s(\vec{Q}_2 - \vec{w}_0)$ the three field operators involved, Eqs.(4),(6) and (7) lead to the 3-mode evolution:

$$\frac{d}{dz} \hat{a}_{0s}(z) = \chi \left[\alpha_1 \hat{b}_i^\dagger(z) + \alpha_2 \hat{c}_i^\dagger(z) \right] e^{-iD(\vec{w}_0)z} \quad (9a)$$

$$\frac{d}{dz} \hat{b}_i(z) = \chi \left[\alpha_1 \hat{a}_{0s}^\dagger(z) \right] e^{-iD(\vec{w}_0)z} \quad (9b)$$

$$\frac{d}{dz} \hat{c}_i(z) = \chi \left[\alpha_2 \hat{a}_{0s}^\dagger(z) \right] e^{-iD(\vec{w}_0)z} \quad (9c)$$

where $D(\vec{w}_0) = \mathcal{D}(\vec{w}_0; \vec{Q}_1) = \mathcal{D}(\vec{w}_0; \vec{Q}_2)$ is the common value of the phase-mismatch. Eqs.(9) can be readily solved by means of a linear transformation acting on the 2 side modes:

$$\begin{pmatrix} \hat{d}_{i+} \\ \hat{d}_{i-} \end{pmatrix} = \begin{pmatrix} \frac{\alpha_1^*}{\bar{\alpha}_p} & \frac{\alpha_2^*}{\bar{\alpha}_p} \\ -\frac{\alpha_2}{\bar{\alpha}_p} & \frac{\alpha_1}{\bar{\alpha}_p} \end{pmatrix} \begin{pmatrix} \hat{b}_i \\ \hat{c}_i \end{pmatrix} \quad (10)$$

where

$$\bar{\alpha}_p = e^{i\frac{\phi_1 + \phi_2}{2}} \sqrt{|\alpha_1|^2 + |\alpha_2|^2}, \quad (11)$$

can be seen as the complex amplitude of a single pump carrying the sum of the energies of the two pumps (ϕ_1, ϕ_2 being the phases of each wave). As it can be immediately verified, the new modes evolve according to:

$$\frac{d}{dz} \hat{a}_{0s}(z) = \chi \bar{\alpha}_p \hat{d}_{i+}^\dagger(z) e^{-iDz} \quad (12a)$$

$$\frac{d}{dz} \hat{d}_{i+}(z) = \chi \bar{\alpha}_p \hat{a}_{0s}^\dagger(z) e^{-iDz}, \quad (12b)$$

while

$$\frac{d}{dz} \hat{d}_{i-}(z) = 0. \quad (13)$$

Eqs.(12) describe a standard PDC process involving modes \hat{a}_{0s} and \hat{d}_{i+} , pumped by a single wave $\bar{\alpha}_p$ of energy $|\bar{\alpha}_p|^2 = |\alpha_1|^2 + |\alpha_2|^2$ and phase $\bar{\phi}_p = \frac{\phi_1 + \phi_2}{2}$. As well known, the solution of Eq.(12), starting from initial conditions

$\hat{a}_{0s}^{in}, \hat{d}_{i+}^{in}$ at the crystal entrance face, are Bogoliubov transformations, which for $D(\vec{w}_0) = 0$ (phase-matched modes) take the form:

$$\begin{aligned}\hat{a}_{0s}(z) &= \cosh(\bar{g}z) \hat{a}_{0s}^{in} + e^{i\bar{\phi}_p} \sinh(\bar{g}z) \hat{d}_{i+}^{in\dagger}, \\ \hat{d}_{i+}(z) &= \cosh(\bar{g}z) \hat{d}_{i+}^{in} + e^{i\bar{\phi}_p} \sinh(\bar{g}z) \hat{a}_{0s}^{in\dagger}.\end{aligned}\quad (14)$$

(the case of arbitrary mismatch can be e.g. found in the Appendix A of Ref.[21], substituting the parameter $\gamma g_0 l_c$ appearing there with $\chi|\bar{\alpha}_p|z$). If instead of the fields, the quantum state is evolved along the medium, the joint state of modes $\hat{a}_{0s}, \hat{d}_{i+}$ is the EPR state (or *two-mode squeezed state*, see e.g. [29]), with squeeze parameter $\chi\bar{\alpha}_p z$. Conversely, mode \hat{d}_{i-} does not evolve along the crystal, and its state remains the same it had at the crystal input (e.g. vacuum or a coherent state): $\hat{d}_{i-}(z) = \hat{d}_{i-}^{in}$.

On the other hand, by inverting the unitary transformation (10) one has $\begin{pmatrix} \hat{b}_i \\ \hat{c}_i \end{pmatrix} = \begin{pmatrix} \frac{\alpha_1}{\bar{\alpha}_p} & -\frac{\alpha_2^*}{\bar{\alpha}_p} \\ \frac{\alpha_2}{\bar{\alpha}_p} & \frac{\alpha_1^*}{\bar{\alpha}_p}, i.e. \end{pmatrix} \begin{pmatrix} \bar{\alpha}_p \\ 0 \end{pmatrix}$, i.e.

$$\begin{pmatrix} \hat{b}_i \\ \hat{c}_i \end{pmatrix} = \begin{pmatrix} e^{i\phi_-} & 0 \\ 0 & e^{-i\phi_-} \end{pmatrix} \begin{pmatrix} \frac{|\alpha_1|}{|\bar{\alpha}_p|} & -\frac{|\alpha_2|}{|\bar{\alpha}_p|} \\ \frac{|\alpha_2|}{|\bar{\alpha}_p|} & \frac{|\alpha_1|}{|\bar{\alpha}_p|} \end{pmatrix} \begin{pmatrix} \hat{d}_{i+} \\ \hat{d}_{i-} \end{pmatrix}\quad (15)$$

where $\phi_- = \frac{\phi_1 - \phi_2}{2}$. It can be immediately recognized that the transformation (15) is equivalent to the action of a lossless beam-splitter, with transmission and reflection coefficients $t = \frac{|\alpha_1|}{|\bar{\alpha}_p|}$ and $r = -\frac{|\alpha_2|}{|\bar{\alpha}_p|}$, respectively. Thus, for each triplet of entangled modes, the doubly pumped PDC scheme can be considered formally equivalent to the sequence shown in Fig.1b, i.e. to:

- i) A standard parametric process, pumped by a single pump of amplitude $\bar{\alpha}_p$, carrying the same total energy of the two pumps, generating a EPR entangled state in modes \hat{a}_{0s} and \hat{d}_{i+} .
- ii) A beam-splitter mixing one of the twin beams generated in step i) with an independent input beam $\hat{d}_{i-} = \hat{d}_{i-}^{in}$; the reflection and transmission of the beam-splitter are in the same ratio as the two pump amplitudes: $\frac{|r|}{|t|} = \frac{\sin\theta}{\cos\theta} = \frac{|\alpha_2|}{|\alpha_1|}$;
- iii) Local phase shifts on the two outputs by the half-difference of the pump phases: $\hat{b}_i, \hat{c}_i \rightarrow \hat{b}_i e^{i\phi_-}, \hat{c}_i e^{-i\phi_-}$.

The two pumps can be in principle derived from a single pump of complex amplitude $\bar{\alpha}_p$, through the same linear transformation described by Eq.(15): $\begin{pmatrix} \alpha_1 \\ \alpha_2 \end{pmatrix} = \begin{pmatrix} e^{i\phi_-} & 0 \\ 0 & e^{-i\phi_-} \end{pmatrix} \begin{pmatrix} \cos\theta & -\sin\theta \\ \sin\theta & \cos\theta \end{pmatrix} \begin{pmatrix} \bar{\alpha}_p \\ 0 \end{pmatrix}$ (also in practice this is a method to obtain the two pump modes[19]). We have shown that the doubly pumped source formally implements the same linear transformation on one of the two parties of an EPR state, where the other mode \hat{d}_{i-} can be in principle externally supplied in any arbitrary state. Such a splitting-mixing can be of relevant practical applications, in protocols of photon-subtracted Gaussian states [10, 11]): the device gives the possibility of redirecting a portion of one party of the EPR state in a separate spatial mode without the need of external alignments, potentially detrimental for the quantum state. The same operations are instead performed on the less fragile classical laser pump.

This tripartite state represents a generalization of the state studied in [12] to arbitrary pump amplitudes: as that one it shows genuine tripartite entanglement, as will be discussed in a separate work [30]. On a different perspective, it is also analogous to the state produced by a nonlinear photonic crystal whose quantum correlations were extensively analyzed in Ref. [21], with the important difference that in the dual pump scheme the splitting ratio $\frac{r}{t} = \frac{|\alpha_2|}{|\alpha_1|}$ can be easily reconfigured, whereas in the NPC case it is fixed by the geometry of the nonlinear grating. A further analogy concerns the presence of hot-spots in the parametric emission at the location of shared and coupled modes, due to the fact that their parametric gain $\bar{g} = \sqrt{g_1^2 + g_2^2}$ is larger than that of the surrounding two-mode fluorescence from pump 1 alone (gain $g_1 = \chi|\alpha_1|$), or pump 2 alone (gain $g_2 = \chi|\alpha_2|$). Therefore in the stimulated regime of PDC where the intensity grows exponentially with the gain, these modes appear as bright spots against a less intense background. This is especially true when the two pumps are balanced, as shown by the simulations in the upper row of Fig.5, performed with two Gaussian pump pulses of equal peak amplitudes. Notice that in these plots all the spectral components within a rather large bandwidth are superimposed, resulting in three continuous branches of hot-spots in the source far-field. According to the results of the plane-wave model, their exponential growth rate along the medium is $\sqrt{2}$ times larger than that of the background conical emission from each pump, in complete analogy with what observed in NPC sources [20, 31, 32]. The case of two strongly unbalanced pumps is illustrated by the second row of Fig.5, where $g_2 = 4g_1$: then, the fluorescence from pump 1 is basically not visible on the scale of the plot, while the left hot-spot branch (corresponding to modes labelled as \hat{b} in the previous section) is visible, although ~ 16 times less intense than the right branch.

A final remark concerns the transformation (10) that decouples the 3-mode evolution, and its connection with the near-field distribution of modes. The simplest case is that of symmetric pump tilts $Q_2 = -Q_1$, in which the transverse

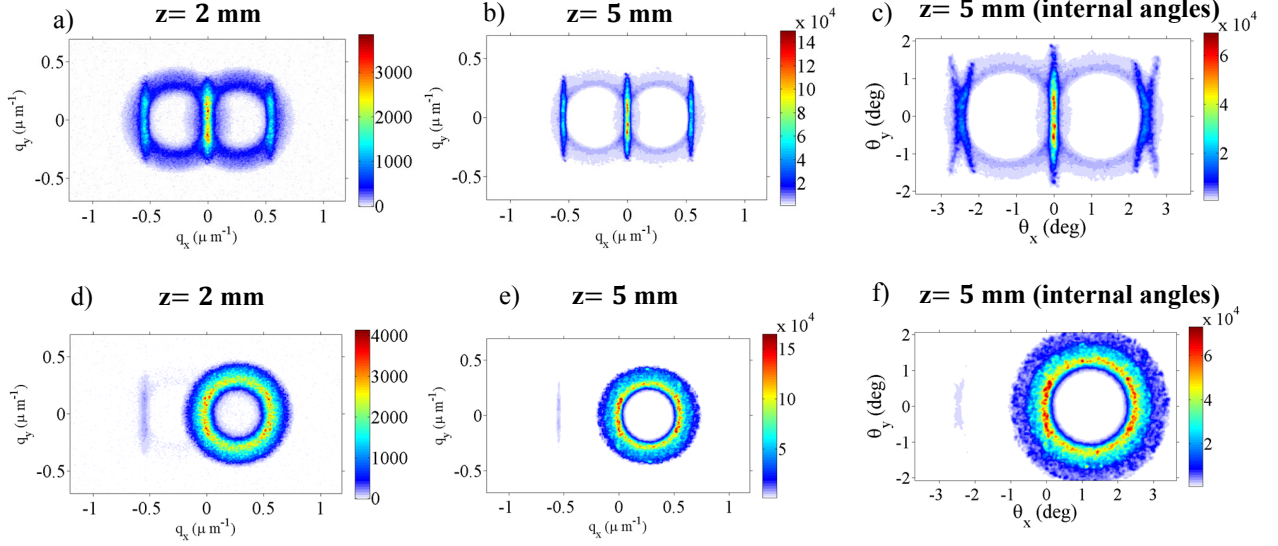


FIG. 5. Numerical simulations of Eq.(1) for a doubly pumped PPLT, showing the Fourier (q_x, q_y) and angular (θ_x, θ_y) intensity distributions of light downconverted in the bandwidth 950 – 1210 nm, from two Gaussian pump pulses of peak amplitudes α_1 and α_2 , 1ps duration and $400 \mu\text{m}$ waist, tilted at $\theta_{p1,p2} = \mp 1.2^\circ$. In the upper row a)-c) $\alpha_2 = \alpha_1$, with the 3 hot-spot branches becoming progressively brighter for increasing propagation length. In the lower row d) - f) $\alpha_2 = 4\alpha_1$, and the left hot-spot branch is much weaker than the right one. The overall peak gain is $\bar{g} = \sqrt{g_1^2 + g_2^2} = 1.2 \text{ mm}^{-1}$, other parameters as in Fig.4.

modulation of the pump occurs along the x axis: $\mathcal{A}_p(x) = \alpha_1 e^{iQ_1 x} + \alpha_2 e^{-iQ_1 x}$ (the general case, in which the pump is modulated along an axis inclined at $\frac{\theta_{p1} + \theta_{p2}}{2}$ is also not difficult to treat). Then, as shown in App.A, shared modes are generated at $q_{0x} = 0$, and because of transverse momentum conservation, the side modes have Fourier coordinates $\vec{q}_b = Q_1 \vec{e}_x$ and $\vec{q}_c = -Q_1 \vec{e}_x$. They generate a transverse field distribution of the form:

$$\hat{b}_i e^{iQ_1 x} + \hat{c}_i e^{-iQ_1 x} = \hat{d}_{i+} u_p(x) + \hat{d}_{i-} u_p^\perp(x), \quad (16)$$

where we used Eq.(15) and $u_p(x) = \frac{\alpha_1 e^{iQ_1 x} + \alpha_2 e^{-iQ_1 x}}{\bar{\alpha}_p}$ can be recognized as the pump spatial mode, such that the pump envelope is $\mathcal{A}_p(x) = \bar{\alpha}_p u_p(x)$. $u_p^\perp(x) = \frac{-\alpha_2^* e^{iQ_1 x} + \alpha_1^* e^{-iQ_1 x}}{\bar{\alpha}_p^*}$ is the orthogonal spatial mode, having the smallest spatial superposition to the pump $\int dx u_p^*(x) u_p^\perp(x) = 0$ ². This makes clear the decomposition in Eq. (10): \hat{d}_{i+} is the spatial mode of the pump, and it is the only one to be parametrically amplified, while \hat{d}_{i-} is the spatial mode orthogonal to the pump and it is not affected by the parametric generation. Notice that the result is less trivial than it might appear: if both the pump modes were not simultaneously phase matched, then it wouldn't hold true.

B. Position of shared and coupled modes

The tripartite entangled state studied in the previous section concerns all the triplets of shared and coupled modes that are solutions of Eq.(8). Their Fourier coordinates are studied in App.A by using the paraxial approximation, and are for example shown by the numerical simulations of Fig.5. These results can be mapped into angles of propagation around the z -axis, $q_x \rightarrow k_s(\Omega) \sin \theta_x \simeq k_s(\Omega) \theta_x$, $q_y \rightarrow k_s(\Omega) \sin \theta_y \simeq k_s(\Omega) \theta_y$, where $k_s(\Omega) \simeq n_e(\omega_s + \Omega, \pi/2) \frac{\omega_s + \Omega}{c}$ ³. We find that shared and coupled modes at the frequency $\omega_s + \Omega$ are generated at angles

$$\theta_{0x}(\Omega) = \frac{\theta_{p1} + \theta_{p2}}{2} \left(1 + \frac{G_z - \mathcal{D}_0(\Omega)}{k_s(\Omega)} \right) \simeq \frac{\theta_{p1} + \theta_{p2}}{2} \quad (17)$$

$$\theta_{b,cx}(\Omega) = \frac{\theta_{p1} + \theta_{p2}}{2} \pm \frac{\theta_{p1} - \theta_{p2}}{2} \frac{k_p}{k_s(\Omega)} \simeq \frac{\theta_{p1} + \theta_{p2}}{2} \pm (\theta_{p1} - \theta_{p2}) \frac{1}{1 + \Omega/\omega_s} \quad (18)$$

² Here we disregard details related to mode normalization and the finite size of the medium, which could be easily fixed by standard methods

³ Notice that when propagating at nearly $\pi/2$ angle with the optical axis, the dependence of n_e on the propagation direction is negligible, especially for LiTaO_3 , whose birefringence is very small [28].

where $\theta_{p1,p2} = \frac{Q_{1,2}}{k_p}$ are the (internal) angles formed by the two pumps with the z -axis, and $\mathcal{D}_0(\Omega) = k_s(\Omega) + k_s(-\Omega) - k_p + G_z$ is the collinear phase-mismatch parameter (i.e. the mismatch one would have if the 3 waves propagated collinearly along the z -axis). As it could be expected, shared modes are approximately emitted in the symmetry plane between the two pumps. This is exactly true when $\theta_{p1} + \theta_{p2} = 0$, i.e. the career of the pump field propagates along z , but approximately holds also when the tilts are not symmetric, because $\frac{G_z}{k_s} \simeq \frac{\lambda_s}{n_e(\lambda_s)\Lambda_{pol}} \approx 0.06$, and $\mathcal{D}_0 \ll k_s$ ⁴. The side modes are approximately displaced by $\pm(\theta_{p1} - \theta_{p2})$ with respect to the shared ones. Examples of triplets of modes are shown in Fig.4, which plots the phase-matching surfaces Σ_1 and Σ_2 in Eq. (5), with shared modes at their intersections. The green dots in Fig.4b show the three entangled modes at the degenerate wavelength, while Figs. 4c and 4d illustrate the case of two conjugate wavelengths out of degeneracy, showing two independent triplets of modes, labelled by dots and stars (notice that at any two conjugate wavelengths there are actually 4 independent triplets of modes).

If the emission frequency is not resolved, the various spectral components of the shared and coupled modes form in the far-field of the source three continuous branches at approximately $\theta_x \simeq \frac{\theta_{p1} + \theta_{p2}}{2}$ (shared modes) and $\theta_x \simeq \frac{\theta_{p1} + \theta_{p2}}{2} \pm (\theta_{p1} - \theta_{p2})$ (coupled modes). These are shown by the numerical simulation in Fig.5, where shared and coupled modes appear as bright bands of hot spots against the less intense background of the 2-mode fluorescence. Notice that these simulations encompass a rather large bandwidth $\Delta\lambda = 260$ nm, so that the angular positions of high and low frequency spectral components split as predicted by Eq. (18).

Most important for our discussion, we notice that for a given finite tilt $\pm(\theta_{p1} - \theta_{p2})$ between the two pumps, the pattern of shared and coupled modes translates rigidly with the angle of propagation $\frac{\theta_{p1} + \theta_{p2}}{2}$ of the career. As a consequence, the position of coupled modes never superimpose to shared ones (stars never superimpose to dots in Fig.4c, d. We will see in Sec. III a different phase-matching configuration, where such a superposition may take place, originating a transition to a 4-mode coupling.

III. TYPE I PROCESS IN BBO: TRANSITION TO A QUADRIPARTITE ENTANGLEMENT

This section studies a second configuration, where the two pump modes propagate inside a standard BBO crystal, forming in general different angles with the optical axis. We shall see that the presence of strong walk-off effects enables a peculiar *resonance* condition, with a transition to a 4-mode entangled state.

We consider the same setup as in the experiment of Ref.[19]. The active material is a BBO crystal, cut for the collinear type I process $e \rightarrow oo$ from $\lambda_p = 352$ nm to $\lambda_s = \lambda_i = 704$ nm. Fig.6 shows the basic geometry: the optical axis O_3 forms an angle $\gamma_0 \simeq 33.44^\circ$ with the mean propagation direction z . Unlike the noncritical phase-matching of Fig.3, two pump modes slightly tilted with respect to z experience in general different refraction indices, because they propagate at different angles γ_1 and γ_2 with the optical axis, and have different wave numbers k_{p1} and k_{p2} , with $k_{pj} = n_e(\omega_p, \gamma_j) \frac{\omega_p}{c}$. The difference $k_{p2} - k_{p1}$ depends not only on the tilt angle, but also on the transverse direction of the tilt. As we shall see in the following, the ability to tune this parameter enables the possibility to achieve the resonance associated to the 4-mode entanglement. Fig.6 A, B and C schematically depict the different geometries, where we associate the direction of the relative tilt between the pumps to the x axis of a reference frame $\{x, y, z\}$ which is allowed to rotate by an angle β in the input facet of the crystal. Notice that in practice the various configurations are realized by implementing a $-\beta$ rotation of the crystal around the z -axis [19].

Then, as shown in App.A [see in particular Eqs.(A14)-(A16)], for a given transverse tilt between the two pumps, the difference of their wave- numbers depends on the rotation β according to the formula (correct up to second order in the small angles θ_p):

$$\frac{\Delta k_p}{\Delta Q_p} = \frac{k_{p2} - k_{p1}}{Q_2 - Q_1} \simeq \rho_\gamma \left(\sin \beta \cos \theta_p \frac{\sin \gamma_0}{\sin \gamma} - \sin \theta_p \frac{\cos \gamma_0}{\sin \gamma} \right) \Big|_{\theta_p = \frac{\theta_{p1} + \theta_{p2}}{2}} \quad (19)$$

$$\rightarrow \begin{cases} \pm \rho_\gamma & \text{for } \beta = \pm \frac{\pi}{2} \\ \rho_0 \left(\sin \beta - \frac{\theta_{p1} + \theta_{p2}}{2} \frac{1}{\text{tg } \gamma_0} \right) & \text{for } |\beta| \ll \frac{\pi}{2} \end{cases} \quad (20)$$

where $\rho_\gamma = -\frac{1}{k_p} \frac{dk_p}{d\gamma}$ is the *walk-off angle* between the wave-vector of the extraordinary wave and its Poynting vector, representing the direction of the energy flux of the wave inside the medium [33, 34]. Here it is calculated at the

⁴ When the tilts are not symmetric, the pump career propagates at a slightly oblique direction with respect to the poling, and in the frame of reference aligned with the pump career, there is a transverse contribution of the reciprocal poling vector.

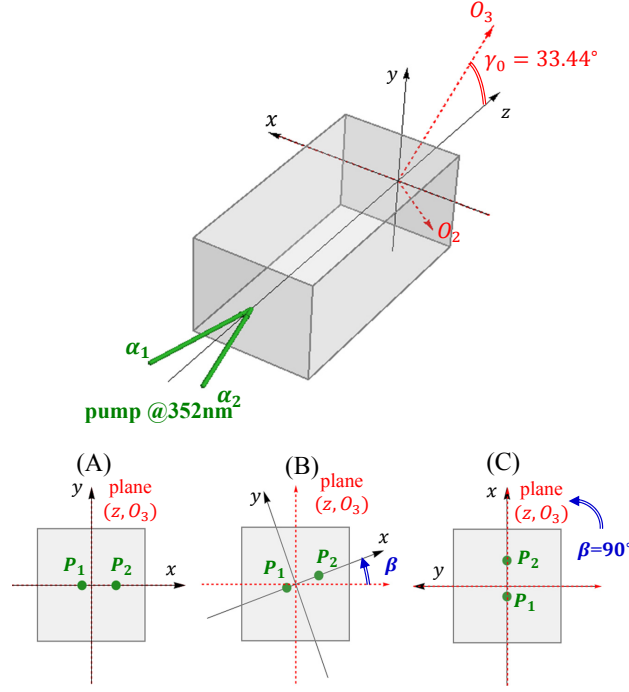


FIG. 6. Geometry of the scheme, for the $e \rightarrow \infty$ process in a BBO crystal, cut at $\gamma_0 = 33.44^\circ$. O_3 is the optical axis. The two pumps propagate mainly along z , with a slight tilt in the x -direction. In the configuration (A) the pumps form roughly the same angle with the optical axis. In (B) and (C) the two pumps propagate at different angles with O_3 , and have different wave-numbers.

angle $\bar{\gamma}$ formed by the carrier wave with the optical axis, but we make a small error in taking it at the cut angle γ_0 , $\rho_{\bar{\gamma}} \rightarrow \rho_0 \simeq 0.0744 \text{ rad} = 4.26^\circ$, according to the Sellmeier relations in Ref. [35]. Clearly $\Delta k_p / \Delta Q_p$ is minimal in the configuration labelled as A in Fig.6 ($\beta = 0$), and it is maximal in the configuration C ($\beta = \pm \frac{\pi}{2}$), where it coincides with the walk-off angle between the carrier wave and its Poynting vector.

A. Shared-coupled modes and transition to resonance

As in the former configuration of Sec.II, each pump generates its own branch of down-converted modes, laying on the phase matching surfaces Σ_1 and Σ_2 defined by Eq.(5). Examples are shown in Fig.7, where the three columns correspond to three different rotation angles β . At difference with the PPLT case of Fig.4, we notice that now the surfaces Σ_1 and Σ_2 have quite different shapes, as discussed in Appendix A, and that their shape changes substantially with β . Actually, for the choice of parameters in this figure, the crystal rotation affects only the phase-matching surface Σ_2 , which changes from non-collinear (Fig.4b) for negative β , to non-degenerate for positive β (Fig.4c).

The geometrical intersections $\bar{\Sigma}_1 \cap \Sigma_2$ determine the position of shared modes $\vec{w}_0 = (q_{0x}, q_{0y}, \Omega_0)$, each of them being coupled to the two modes $\vec{w}_b = (Q_1 - q_{0x}, -q_{0y}, -\Omega_0)$ and $\vec{w}_c = (Q_2 - q_{0x}, -q_{0y}, -\Omega_0)$. Their Fourier coordinates are determined by Eq.(8), and are studied in Appendix A [see Eqs. (A7)-(A10)]. By translating these results into propagation angles around the z axis, and neglecting infinitesimal terms $\frac{\mathcal{D}_0(\Omega)}{k_p} \ll 1$ ⁵ we find that the angular positions of shared and coupled modes are given by

$$\theta_{0x}(\Omega) = \frac{\theta_{p1} + \theta_{p2}}{2} + \frac{\Delta k_p}{\Delta Q_p} \frac{k_s(-\Omega)}{k_s(\Omega)} \quad (21)$$

$$\theta_{b,cx}(\Omega) = \frac{\theta_{p1} + \theta_{p2}}{2} \pm \frac{\theta_{p1} - \theta_{p2}}{2} \frac{k_p}{k_s(\Omega)} - \frac{\Delta k_p}{\Delta Q_p}, \quad (22)$$

⁵ $\frac{\mathcal{D}_0(\Omega)}{k_p} < 10^{-2}$ for wavelengths in the whole interval $0.43\text{-}2.1 \mu\text{m}$

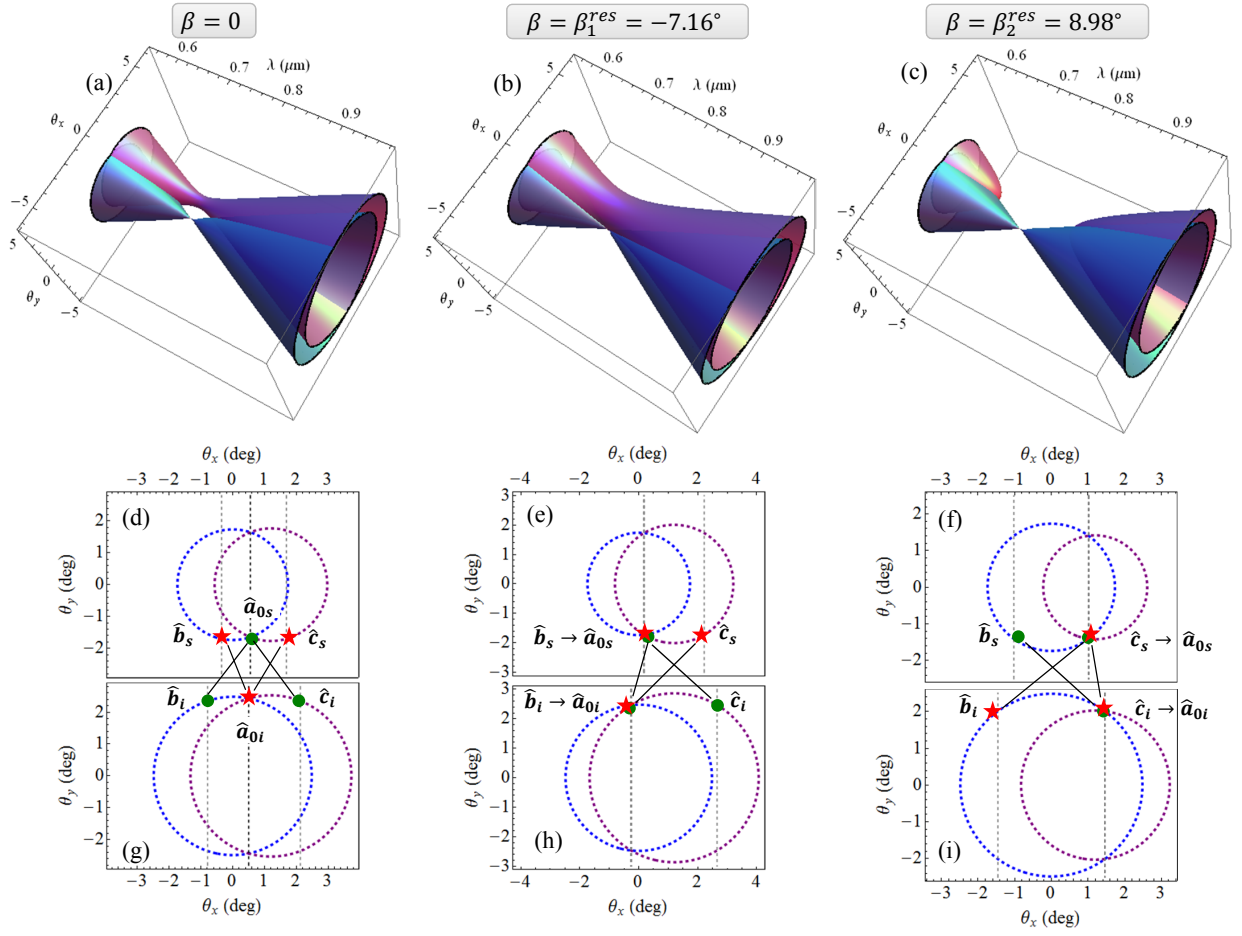


FIG. 7. BBO doubly pumped at 352nm. $\theta_{p1} = 0; \theta_{p2} = 1.2^\circ$. (a,b,c) Surfaces in the $(\lambda, \theta_x, \theta_y)$ space defining phase-matching for the two pumps [see Eq.(5)], calculated with the Sellmeier formulas in [35]. (d-i) Angular phase-matching curves at the two conjugate wavelengths $\lambda_s = 0.6 \mu\text{m}$ (d,e,f) and $\lambda_i = 0.85 \mu\text{m}$ (g,h,i), illustrating the transition to resonance. The symbols show the position of shared and coupled modes. For $\beta = 0$ (left column) two independent triplets of entangled modes coexist (dots and stars). At $\beta_1^{res} = -7.16^\circ$ (central column) and $\beta_2^{res} = 9.98^\circ$ (right column), resonance is achieved. The two triplets of modes merge into four entangled modes

while in the y-direction $\theta_{0y}(\Omega) = \theta_{b,cy}(\Omega)$. In comparison with the noncritical phase-matching of Sec.II [see Eqs. (17) and (18)] we here see the presence of additional terms $\propto \frac{\Delta k_p}{\Delta Q_p}$, which have the effect of shifting the angular positions of shared and coupled modes in opposite directions. Thus, by continuously varying this parameter, one of the side modes may arrive to superimpose to the central shared mode at the same frequency, to which it was originally uncoupled, thus becoming itself shared. As it can be easily verified, the condition $\theta_{b,c}(\Omega) = \theta_0(\Omega)$ takes place for

$$\frac{\Delta k_p}{\Delta Q_p} \left(1 + \frac{\mathcal{D}_0(\Omega)}{k_p} \right) \simeq \frac{\Delta k_p}{\Delta Q_p} = \begin{cases} \frac{\theta_{p1} - \theta_{p2}}{2} & \theta_0(\Omega) = \theta_b(\Omega) \\ \frac{\theta_{p2} - \theta_{p1}}{2} & \theta_0(\Omega) = \theta_c(\Omega) \end{cases} \quad (23)$$

where again we neglected $\frac{\mathcal{D}_0(\Omega)}{k_p} \ll 1$. According to the results in Eq.(19), we notice that such conditions can be reached for any value of the tilt angle between the pumps smaller than the walk-off angle, by properly adjusting the transverse rotation of the crystal.

We call the conditions in Eq.(23) *resonances*, because of their striking analogy with the resonance that was observed in nonlinear photonic crystals [20, 21] by tilting the direction of a single pump wave inside the nonlinear grating. As for the NPC, at resonance two triplets of modes, originally uncoupled merge into a group a four modes, whose joint state is the quadripartite entangled state that will be described in Sec.III B. Moreover, as demonstrated by the experiment of Ref.[19], at resonance the parametric gain of hot-spots undergoes a *Golden Ratio* enhancement, again in perfect analogy with what observed in a hexagonally poled NPC [20].

Fig.7 provides an example of the transition to resonance, for the two conjugate wavelengths $\lambda_s = 0.6\mu\text{m}$ and $\lambda_i = 0.85\mu\text{m}$. In first column $\beta = 0$, and the configuration is analogue to the one studied in Sec.II: dots and the stars correspond to two independent triplets of modes, which evolve according to the 3-mode propagation equation (9), and whose state is the tripartite entangled state described in Sec.II A. In the second and third columns $\sin(\beta) = \pm \frac{\theta_{p1} - \theta_{p2}}{2\rho_0} + \frac{\theta_{p2} + \theta_{p1}}{2 \text{tg } \gamma_0}$, respectively, corresponding to the two resonance conditions in Eq.(23)[See also Eq. (A19)]. At $\beta = -7.16^\circ$, all the shared modes merge with the left branch of coupled modes, generated by pump 1: $\hat{a}_{0s}, \hat{a}_{0i} \rightarrow \hat{b}_s, \hat{b}_i$. At $\beta = 8.98^\circ$ the merging takes place between shared modes and the right branch of coupled modes, generated by pump 2: $\hat{a}_{0s}, \hat{a}_{0i} \rightarrow \hat{c}_s, \hat{c}_i$.

Remarkably, resonance is achieved simultaneously for all shared-coupled modes in a huge bandwidth around the degenerated wavelength. Indeed, even though the position of shared-coupled modes depends on the frequency, the resonance condition does not: for any practical purpose, the term $\frac{\mathcal{D}_0(\Omega)}{k_p}$ in Eq. (23) can be neglected because $\frac{\mathcal{D}_0(\Omega)}{k_p} \simeq \frac{\Omega^2}{\Omega_B^2}$, where $\Omega_B = \sqrt{\frac{k_p}{k'_s}} \approx 2 \times 10^{16} \text{ s}^{-1}$.

Finally, the meaning of the resonance can be also appreciated by reformulating Eq.(23) in terms of Fourier modes, for which resonance is achieved when $\vec{q}_0(\Omega) = \vec{q}_{b,c}(\Omega) = \vec{Q}_{1,2} - \vec{q}_0(-\Omega)$. This implies

$$\vec{q}_0(\Omega) + \vec{q}_0(-\Omega) = \begin{cases} \vec{Q}_1 \\ \vec{Q}_2 \end{cases} \quad (24)$$

where the upper (lower) condition corresponds to the upper (lower) condition in Eq.(23). Eq.(24) is nothing else than the conservation of transverse momentum involving one pump mode and the two shared modes: as a consequence, at resonance, shared modes at any two conjugate wavelengths, otherwise uncoupled, become populated by photons pairs originating from the same pump mode. We notice that when one of the above conditions holds, not only shared modes superimpose to one branch of coupled modes, but also they become approximately collinear in the x-direction to one of the pump modes, as can be easily checked from Eq.(21) (see also the examples in Fig.7),

B. Quadripartite entanglement

This section studies the quadripartite entangled state generated at resonance. Let us concentrate for definiteness on the upper resonance condition in Eq.(23), at which two shared modes \vec{w}_0 and \vec{w}'_0 become coupled via the pump 1, thus satisfying $\vec{w}_0 + \vec{w}'_0 = \vec{Q}_1$. The results for the other resonance can be obtained by exchanging $\hat{b}_s, \hat{b}_i \leftrightarrow \hat{c}_s, \hat{c}_i$ and $g_1 \leftrightarrow g_2$.

Figs.7e) and h) show the schematics of the coupling in this case. Focusing on a specific pair of conjugate frequencies $\pm\Omega_0$, labeled by subscripts s and i , the coupling involves the following four modes:

$$\text{shared modes} \begin{cases} \hat{b}_s := \hat{A}_s(\vec{w}_0) \\ \hat{b}_i := \hat{A}_s(\vec{Q}_1 - \vec{w}_0) \end{cases} \quad \text{coupled modes} \begin{cases} \hat{c}_s := \hat{A}_s(\vec{Q}_2 - \vec{Q}_1 + \vec{w}_0) \\ \hat{c}_i := \hat{A}_s(\vec{Q}_2 - \vec{w}_0) \end{cases} \quad (25)$$

Their evolution equations read

$$\begin{aligned} \frac{d\hat{b}_s}{dz} &= \left[g_1 \hat{b}_i^\dagger + g_2 \hat{c}_i^\dagger \right] e^{-iD(\vec{w}_0)z} \\ \frac{d\hat{c}_s}{dz} &= \left[g_2 \hat{b}_i^\dagger \right] e^{-iD(\vec{w}_0)z} \\ \frac{d\hat{b}_i}{dz} &= \left[g_1 \hat{b}_s^\dagger + g_2 \hat{c}_s^\dagger \right] e^{-iD(\vec{w}_0)z} \\ \frac{d\hat{c}_i}{dz} &= \left[g_2 \hat{b}_s^\dagger \right] e^{-iD(\vec{w}_0)z} \end{aligned} \quad (26)$$

where the coupling coefficients $g_1 = \chi_1 \alpha_1$ and $g_2 = \chi_2 \alpha_2$ are proportional to the pump amplitudes, but may also include a small effect due to the different nonlinear response of the medium in the two pump directions. The parameter $D(\vec{w}_0) = D(\vec{w}_0, \vec{Q}_1) = D(\vec{w}_0, \vec{Q}_2) = D(\vec{w}_0, \vec{Q}_2 - \vec{Q}_1)$ is the common value of the phase-mismatch, that must be assumed small.

If one prefers the quantum state picture, then the evolution law of the state associated to a quadruplet of modes is easily found in the simplest case of perfect phase-matching. For $D = 0$, the propagation equations (26) can be recast

as $\frac{d\hat{O}}{dz} = \frac{1}{i\hbar} [\hat{\mathcal{P}}, \hat{O}]$, where $\hat{O} = \hat{b}_s \dots \hat{c}_i$, and the "momentum" operator is $\hat{\mathcal{P}} = -i\hbar [g_1 \hat{b}_s^\dagger \hat{b}_i^\dagger + g_2 (\hat{b}_s^\dagger \hat{c}_i^\dagger + \hat{c}_s^\dagger \hat{b}_i^\dagger) - \text{h.c.}]$. Then the state evolves according to

$$\begin{aligned} |\psi\rangle_{out} &= e^{\frac{i}{\hbar} \hat{\mathcal{P}} z} |\psi\rangle_{in} \\ &= e^{[g_1 \hat{b}_s^\dagger \hat{b}_i^\dagger + g_2 (\hat{b}_s^\dagger \hat{c}_i^\dagger + \hat{c}_s^\dagger \hat{b}_i^\dagger) - \text{h.c.}] z} |\psi\rangle_{in} \end{aligned} \quad (27)$$

$$\xrightarrow{\bar{g}z \rightarrow 0} |\psi\rangle_{in} + z \left[g_1 \hat{b}_s^\dagger \hat{b}_i^\dagger + g_2 (\hat{b}_s^\dagger \hat{c}_i^\dagger + \hat{c}_s^\dagger \hat{b}_i^\dagger) \right] |\psi\rangle_{in} \quad (28)$$

where in writing Eq.(27) we assumed some form of discretization of Fourier modes (details not relevant to our discussion). Eqs. (27) or (28) show the two-photon processes occurring in the quadruplet of modes: a photon pair may be down-converted from pump 1, with probability amplitude $g_1 \propto \alpha_1$, and appear in modes \hat{b}_s, \hat{b}_i . Alternatively, paired photons can be generated from pump 2 (probability amplitude $g_2 \propto \alpha_2$) and appear in one of the two couples (\hat{b}_s, \hat{c}_i) or (\hat{c}_s, \hat{b}_i). When one of the two pumps is absent, the state reduces to a product of bipartite EPR states generated by each pump; for example, for $g_1 = 0$ the equations show the contribution of two independent couples of entangled modes over the many couples generated by down-conversion from pump 2.

As for any multipartite Gaussian entangled state [36], the quadripartite state in Eq.(27) can be decomposed into 4 single-mode squeezed states mixed by passive linear transformations. In our case, we prefer a decomposition into a pair of bipartite EPR states (each of them can be in turn thought of as the balanced interference of two squeezed states). This decomposition is accomplished by the following linear transformation acting separately on the signal and idler modes

$$\begin{pmatrix} \hat{b}_j \\ \hat{c}_j \end{pmatrix} = \underline{\underline{\mathbf{U}}} \begin{pmatrix} \hat{\sigma}_j \\ \hat{\delta}_j \end{pmatrix} \quad (j = s, i), \quad (29)$$

$$\underline{\underline{\mathbf{U}}} = \begin{pmatrix} e^{i\frac{\phi_1}{2}} & 0 \\ 0 & e^{i\frac{\phi_2}{2}} e^{-i\phi_-} \end{pmatrix} \cdot \begin{pmatrix} \cos \theta & \sin \theta \\ -\sin \theta & \cos \theta \end{pmatrix} \quad (30)$$

where the mixing coefficients $\cos \theta$ and $\sin \theta$ depend on the ratio between the two pump intensities, as described by Eq.(35) and shown by Fig.8b. Under this transformation the equations (26) decouples into two independent standard

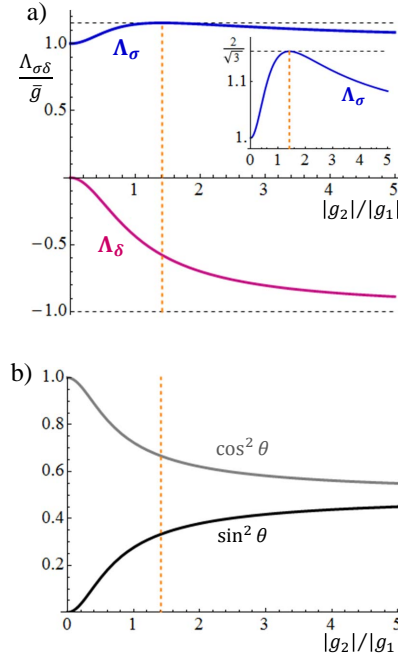


FIG. 8. a) Squeeze eigenvalues Λ_σ and Λ_δ in Eq.(34), normalized to the reference squeeze parameter \bar{g} of a single pump carrying all the energy. The inset shows the maximum of Λ_σ , occurring at $|g_2| = \sqrt{2}|g_1|$. b) Mixing coefficients of the unitary transformation in Eq.(30)

parametric processes of the form

$$\begin{aligned}\frac{d}{dz}\hat{\delta}_s(z) &= \Lambda_\delta \hat{\delta}_i^\dagger(z)e^{-iDz} \\ \frac{d}{dz}\hat{\delta}_i(z) &= \Lambda_\delta \hat{\delta}_s^\dagger(z)e^{-iDz}\end{aligned}\quad (31)$$

and

$$\begin{aligned}\frac{d}{dz}\hat{\sigma}_s(z) &= \Lambda_\sigma \hat{\sigma}_i^\dagger(z)e^{-iDz} \\ \frac{d}{dz}\hat{\sigma}_i(z) &= \Lambda_\sigma \hat{\sigma}_s^\dagger(z)e^{-iDz}\end{aligned}\quad (32)$$

Both the squeeze parameters Λ_σ , Λ_δ and the mixing coefficients of the unitary $\underline{\mathbf{U}}$ depend only on the ratio

$$\rho = \frac{|g_2|}{|g_1|} \propto \frac{|\alpha_2|}{|\alpha_1|}, \quad (33)$$

according to the following equations:

$$\Lambda_{\sigma\delta} = |g_1|f_\pm(\rho) = \frac{\bar{g}}{\sqrt{1+\rho^2}}f_\pm(\rho) \quad (34)$$

$$\cos\theta = \frac{f_+(\rho)}{\sqrt{\rho^2 + f_+^2(\rho)}}, \quad \sin\theta = -\frac{\rho}{\sqrt{\rho^2 + f_+^2(\rho)}} \quad (35)$$

$$f_\pm(\rho) = \frac{1 \pm \sqrt{1+4\rho^2}}{2}.$$

In these formulas $\bar{g} = \sqrt{|g_1|^2 + |g_2|^2}$ is the reference squeeze parameter, corresponding to standard PDC pumped by a single beam carrying the total energy of the two modes (apart from minor corrections arising from different nonlinear coefficients).

Under the same transformation the output state reduces to the product of two independent EPR states in modes $\hat{\sigma}_j$ and $\hat{\delta}_j$, $|\psi\rangle_{out} \rightarrow e^{[\Lambda_\sigma \hat{\sigma}_s^\dagger \hat{\sigma}_i^\dagger - \text{h.c.}]z} e^{[\Lambda_\delta \hat{\delta}_s^\dagger \hat{\delta}_i^\dagger - \text{h.c.}]z} |\psi\rangle_{in}$. Figure 2 shows the unfolding of the state: the 4-mode entangled state generated at resonance is formally equivalent to: i) *two* nonlinear processes, each generating an EPR pair with squeeze parameters Λ_σ and Λ_δ ; followed by ii) a beam splitter with transmission and reflection coefficients $t = \cos\theta$ and $r = \sin\theta$, respectively, which mixes the two EPR pairs, and iii) phase rotations in the two output arms, by $\frac{\phi_1}{2}$ and $\frac{\phi_2}{2} - \phi_-$, respectively. We remark that the splitting ratio r/t of the beam-splitter can be varied by modulating the pump intensities [Eq.(35)], which means the scheme is potentially able to produce any arbitrary mixing of a pair of EPR states, offering in this way the possibility of engineering the 4-mode entanglement.

A quantitative characterization of the entanglement of this state is outside the scopes of this work and will be performed elsewhere [30]. We simply notice that all the modes interact in a linear chain, shown e.g. by the scheme in Fig. 7e,h. Their genuine quadripartite entanglement can be demonstrated by noticing that there exist four independent combinations of mode quadrature operators whose variances vanish in the limit of large squeezing, violating thus any bound imposed by separability. Precisely, by defining the quadrature operators of modes \hat{b}_j relative to the phase of pump 1, i.e. $\hat{X}_{b_j} = \hat{b}_j e^{-i\frac{\phi_1}{2}} + \hat{b}_j^\dagger e^{+i\frac{\phi_1}{2}}$, defining those of modes c_j as $\hat{X}_{c_j} = \hat{c}_j e^{-i\frac{\phi_2}{2}} e^{i\phi_-} + \hat{c}_j^\dagger e^{+i\frac{\phi_2}{2}} e^{-i\phi_-}$, by using the inverse of transformation (30) and the standard properties of EPR states, it can be shown that

$$\begin{aligned}\hat{f}_I &= \cos\theta(\hat{X}_{b_s} - \hat{X}_{b_i}) - \sin\theta(\hat{X}_{c_s} - \hat{X}_{c_i}) = \sqrt{2}e^{-\Lambda_\sigma z} \hat{X}_I(0) \\ \hat{f}_{II} &= \sin\theta(\hat{X}_{b_s} + \hat{X}_{b_i}) + \cos\theta(\hat{X}_{c_s} + \hat{X}_{c_i}) = \sqrt{2}e^{-|\Lambda_\delta|z} \hat{X}_{II}(0),\end{aligned}\quad (36)$$

where $\hat{X}_I(0)$ and $\hat{X}_{II}(0)$ are independent input operators that can be taken in the vacuum state. At the same time for the orthogonal quadratures \hat{Y}_α , such that $[\hat{X}_\alpha, \hat{Y}_\beta] = 2i\delta_{\alpha,\beta}$, ($\alpha, \beta = b_s..c_i$), one can show that

$$\begin{aligned}\hat{f}_{III} &= \cos\theta(\hat{Y}_{b_s} + \hat{Y}_{b_i}) - \sin\theta(\hat{Y}_{c_s} + \hat{Y}_{c_i}) = \sqrt{2}e^{-\Lambda_\sigma z} \hat{Y}_{III}(0) \\ \hat{f}_{IV} &= \sin\theta(\hat{Y}_{b_s} - \hat{Y}_{b_i}) + \cos\theta(\hat{Y}_{c_s} - \hat{Y}_{c_i}) = \sqrt{2}e^{-|\Lambda_\delta|z} \hat{Y}_{IV}(0)\end{aligned}\quad (37)$$

where again $\hat{Y}_{III}(0)$ and $\hat{Y}_{IV}(0)$ are independent vacuum operators. The observables $\hat{f}_I, \dots, \hat{f}_{IV}$ commute pairwise, so that in general there is no lower bound for their variances. However, in the same spirit of [37, 38], it is possible to formulate bounds that must be satisfied by states separable with respect to any specific bipartition, which are violated when the gain $\bar{g}z$ is large enough, provided that both $|\alpha_1| \neq 0$ and $|\alpha_2| \neq 0$ [30].

Interestingly, the bigger squeeze eigenvalue is always slightly larger than \bar{g} , and presents a maximum at $|g_2| = \sqrt{2}|g_1|$, i.e. when the pump 2 is approximately twice as intense as pump 1, where $\Lambda_\sigma = \frac{2}{\sqrt{3}}\bar{g} \simeq 1.15\bar{g}$. This means that at resonance the doubly pumped scheme achieves a larger amount of squeezing/gain in the auxiliary modes $\hat{\sigma}_j$ with respect to a standard single-pump scheme, at the same level of injected energy. In this way squeezing/entanglement is concentrated in specific modes.

Finally, we notice that for $\rho = 1$, i.e. when the two pump intensities are balanced, the squeeze eigenvalues reduce to $\Lambda_\sigma = |g_1|\Phi$ and $\Lambda_\delta = -\frac{|g_1|}{\Phi}$ where $\Phi = \frac{1+\sqrt{5}}{2}$ is the Golden Ratio: in this case the doubly pumped PDC scheme realizes a complete analogy with the "Golden Ratio Entanglement" demonstrated in a hexagonally poled photonic crystal [21] with a single pump. An interesting comparison is also with the quadripartite entanglement generated in a *doubly* pumped nonlinear photonic crystal [15]: in this case the squeeze eigenvalues are controlled not only by the relative intensity but also by the relative *phase* of the two pumps, which allows to access a larger variety of states. .

C. The resonance and the Poynting vectors

The resonance, as we called the transition from 3 to 4-mode entanglement, admits an interesting interpretation in terms of a superposition between the Poynting vector of the pump career, representing the mean direction of propagation of the energy flux, and one of the pump modes. This interpretation is particularly evident in the configuration C of Fig.6, and is illustrated in Fig.9. In this case, the

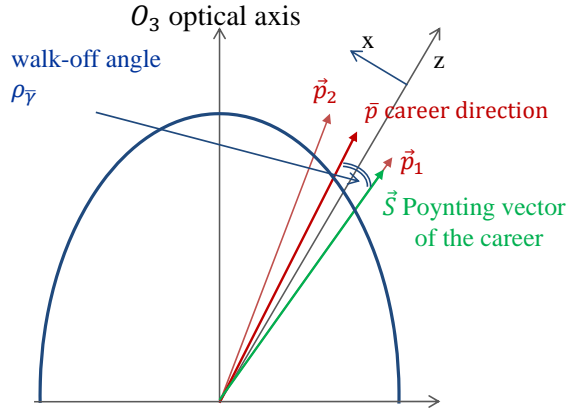


FIG. 9. Illustration of the resonance in the case $\beta = \frac{\pi}{2}$. The blue thick line represents the ellipsoid of the refractive indexes, \vec{p}_1 , \vec{p}_2 and \vec{p} show the directions of propagation of pump 1, pump2, and of the pump career respectively, while \vec{S} is the propagation direction of its Poynting vector. At resonance, it superimposes to the direction of propagation of pump 1

problem becomes 2-dimensional because the pump modes share the same principal plane, which includes the optical axis O_3 . The wave-vector of the pump career lies at an angle $\frac{\theta_{p2} + \theta_{p1}}{2}$ from the z-axis, and its Poynting vector walks-off in the principal plane by an amount ρ_γ , away from the optical axis (BBO is a negative uniaxial crystal), i.e. it forms an angle $\theta_{\vec{S}} = \frac{\theta_{p2} + \theta_{p1}}{2} - \rho_\gamma$ with the z-axis. For $\beta = \frac{\pi}{2}$, the resonance conditions, described by Eq.(23) and Eq.(19), reduce to $\rho_\gamma = \mp \frac{\theta_{p2} - \theta_{p1}}{2}$. For our choice of parameters $\theta_{p2} - \theta_{p1} > 0$, and only the lower condition can be satisfied, leading to $\theta_{\vec{S}} = \theta_{p1}$. For $\beta = -\frac{\pi}{2}$ the roles of p1 and p2 are exchanged (the x axis is reversed), leading to

$$\theta_{\vec{S}} = \begin{cases} \theta_{p2} & \text{for } \beta = -\frac{\pi}{2} \\ \theta_{p1} & \text{for } \beta = +\frac{\pi}{2} \end{cases} \quad (38)$$

i.e. to the result that the resonance condition exactly corresponds to the superposition between the direction of propagations of the Poynting vector of the career and one of the pump modes.

The general case is slightly more involved, because of the full 3-dimensional geometry of the problem. It becomes quite clear when the pump tilts are symmetric, i.e. the pump career propagates along z. Then its Poynting vector points

as in Fig.9 and the resonance condition becomes $\rho_0 \sin \beta = \mp \frac{\theta_{p2} - \theta_{p1}}{2}$. For $\beta = 0$ the plane (\vec{p}_2, \vec{p}_1) is perpendicular to the plane of the figure, and there is no possibility of superposition. For $\beta \neq 0$, the transverse component of the Poynting vector in the x direction of the tilt can superimpose to one of the pump modes, allowing thus a resonance.

IV. CONCLUSIONS

This work has analysed two doubly pumped schemes of parametric down-conversion, in realistic experimental configurations, which exploit standard and commercially available nonlinear media. It has highlighted a stringent analogy with the phenomena predicted and observed in 2-dimensional nonlinear photonic crystals, by using simpler sources which do not need lengthy poling procedures, and offering in addition the possibility of reconfiguring some properties of the state by a simple modulation of the classical laser beam driving the process.

In the non-critical phase-matching case of the PPLT our analytical results, complemented by numerical simulation, may constitute a proposal for future experimental implementations. In our opinion the main outcome here concerns the possibility of implementing an arbitrary beam-splitter on one of two parties of the EPR state generated by standard parametric down-conversion by acting on the spatial structure of the classical laser beam rather than on the fragile quantum state.

The BBO case has already found an experimental demonstration for what concerns the classical properties of the process [19]. For the quantum properties, the highlight result is the possibility of directly generating quadripartite entangled states, and of modulating their properties by acting on the intensities of the two pump modes. This possibility is enabled by the walk-off effects present in such an anisotropic material, in a way that is in our opinion highly nontrivial. In particular, the 4-mode entanglement can be realized at any small tilt angles between the pumps (namely provided that the tilt angle is smaller than the walk-off angle in the central direction of light propagation). We offered also an interpretation of the resonance, as we called the transition from 3- to 4-mode entanglement, in terms of a superposition between the career Poynting vector, which identifies the direction of propagation of the energy flux, with either one pump mode or the other.

Appendix A: Analytical calculations in paraxial approximation

This Appendix summarizes some analytic results, derived by using the paraxial approximation. The dependence on the frequency Ω is maintained till the very end, because we are interested in large emission bandwidths. Precisely, the z -component of the signal wave-vector is approximated as:

$$k_{sz}(\vec{q}, \Omega) = \sqrt{k_s^2(\Omega) - q^2} \rightarrow k_s(\Omega) - \frac{q^2}{2k_s(\Omega)} \quad (\text{A1})$$

valid for $q \ll k_s(\Omega)$ (small angles around the z). The wave-number $k_s(\Omega)$ does not depend on the propagation direction because a) in the PPLT case the down-converted light propagates close to $\frac{\pi}{2}$ (and the material has a very small birefringence), and b) in the BBO case the signal is an ordinary wave. For the extraordinary pump waves:

$$k_{pzj} = \sqrt{k_{pj}^2 - Q_j^2} \simeq k_{pj} - \frac{Q_j^2}{2k_p} \quad (j = 1, 2) \quad (\text{A2})$$

where $k_p = n_e(\omega_p, \gamma_0) \frac{\omega_p}{c}$, and: a) in the PPLT case $k_{pj} = k_p$; b) in the BBO case $k_{pj} = n_e(\omega_p, \gamma_j) \frac{\omega_p}{c}$ depends on the angle γ_j formed by the wave with the optical axis O_3 . Let us consider the geometry in Fig.6, where the transverse tilt of the pump takes place along the x -direction, inclined at an angle β in the input facet of the crystal. In the reference frame (x', y', z) parallel to the facets of the crystal [not to be confused with the crystalline reference frame (O_1, O_2, O_3)], the versors associated with the direction of propagation of a generic pump wave and with the optical axis O_3 are respectively:

$$\frac{\vec{k}_p}{k_p} = \begin{pmatrix} \sin \theta_p \cos \beta \\ \sin \theta_p \sin \beta \\ \cos \theta_p \end{pmatrix}, \quad \vec{e}_3 = \begin{pmatrix} 0 \\ \sin \gamma_0 \\ \cos \gamma_0 \end{pmatrix} \quad (\text{A3})$$

The angle formed by the pump with the optical axis is thus determined by

$$\cos \gamma = \frac{\vec{k}_p \cdot \vec{e}_3}{k_p} = \cos \theta_p \cos \gamma_0 + \sin \theta_p \sin \gamma_0 \sin \beta. \quad (\text{A4})$$

For small pump tilts, the variation of γ with θ_p is minimal for $\beta = 0$ (as in Fig.6A), where $\cos \gamma \simeq \cos \gamma_0(1 - \frac{\theta_p^2}{2})$, while it is maximal for $\beta = \pm 90^\circ$, where $\gamma = \gamma_0 \mp \theta_p$.

Phase matching surfaces

By inserting the approximated expressions (A1) and (A2) into the definition of the phase matching function in Eq. (2), and performing some long but simple algebra, the equation for the phase matching surfaces Σ_1 and Σ_2 defined in Eq. (5) can be obtained as:

$$\left| \vec{q} - \vec{Q}_j \frac{k_s(\Omega)}{k_s(\Omega) + k_s(-\Omega)} \right|^2 = F_j(\Omega) \quad (j = 1, 2), \quad (\text{A5})$$

$$F_j(\Omega) = \bar{k}(\Omega) \left[\mathcal{D}_0(\Omega) - (k_{pj} - k_p) + \frac{\vec{Q}_j^2}{k_p} \frac{\mathcal{D}_0(\Omega) - G_z}{k_p + \mathcal{D}_0(\Omega) - G_z} \right] \quad (\text{A6})$$

where $\bar{k}(\Omega) = \frac{2k_s(\Omega)k_s(-\Omega)}{k_s(\Omega) + k_s(-\Omega)}$, and $\mathcal{D}_0(\Omega) = k_s(\Omega) + k_s(-\Omega) - k_p + G_z$ is the collinear phase-mismatch function. In Eq.(A6) one must take: a) $G_z \neq 0$ and $k_{pj} - k_p = 0$ for the PPLT; b) $G_z = 0$ for the BBO (poling is absent). For the frequencies such that $F_j(\Omega) > 0$, Eq. (A5) represents a family of circumferences, centered around $q_{jx}^c(\Omega) = Q_j \frac{k_s(\Omega)}{k_s(\Omega) + k_s(-\Omega)} \simeq \theta_{pj} k_s(\Omega)$. Thus the angular coordinate of the center is approximately $q_{jx}^c(\Omega)/k_s(\Omega) \simeq \theta_{pj}$. As expected, the two emission branches are conical surfaces roughly collinear with each pump, examples being shown in figures 4 and 7. The shape of each surface depends on the value of $F_j(\Omega = 0)$ in the standard way, i.e. it is an open tube for $F_j(0) > 0$, which collapses to a "hourglass" for $F_j(0) = 0$, while it presents two separate branches for $F_j(0) < 0$. Notice that in the PPLT case the shape changes slowly with the tilt angle, so that the two phase-matching branches look very similar (see Fig. 4), while in the BBO case it has a much faster variation due to the term $k_{pj} - k_p$, so that in general Σ_1 and Σ_2 look quite different (see Fig. 7).

Shared and coupled modes.

The Fourier coordinates of shared modes and of their coupled ones is determined by Eq.(8). By imposing the shared mode condition $\mathcal{D}(\vec{w}_0; \vec{Q}_1) = \mathcal{D}(\vec{w}_0; \vec{Q}_2)$, using again Eqs (A1) and (A2), and reordering the various terms, one obtains the following condition on the x-component of the wave- vector:

$$q_{0x}(\Omega) = \frac{Q_1 + Q_2}{2} \left(1 - \frac{k_s(-\Omega)}{k_p} \right) + \frac{\Delta k_p}{\Delta Q_p} k_s(-\Omega) \quad (\text{A7})$$

where

$$\frac{\Delta k_p}{\Delta Q_p} = \frac{k_{p2} - k_{p1}}{Q_2 - Q_1} \quad (\text{A8})$$

measures the rate of variation of the pump wave-numbers with their transverse tilts. Such a term is absent in the PPLT scheme, but plays a crucial role in the BBO case because of the strong birefringence of the material. The y-component of the wave-vector is obtained by requiring that phase matching is satisfied, i.e. that $\mathcal{D}(\vec{w}_0; \vec{Q}_1) = \mathcal{D}(\vec{w}_0; \vec{Q}_2) = 0$. Using Eq. (A5), one has

$$q_{0y}(\Omega) = \pm \sqrt{F_j(\Omega) - [q_{0x} - q_x^c]^2} \quad (\text{A9})$$

for $F_j(\Omega) - [q_{0x} - q_x^c]^2 \geq 0$, i.e. provided that the intersection between Σ_1 and Σ_2 exists. The \pm signs correspond to the two possible intersection points of two circumferences.

The modes coupled to each shared mode have equation $\vec{q}_b(\Omega) = \vec{Q}_1 - \vec{q}_0(-\Omega)$ (via pump 1) and $\vec{q}_c(\Omega) = \vec{Q}_2 - \vec{q}_0(-\Omega)$ (via pump 2). At a given frequency Ω , their transverse coordinates are:

$$\begin{aligned} q_{b,cx}(\Omega) &= Q_{1,2} - \frac{Q_1 + Q_2}{2} \left(1 - \frac{k_s(\Omega)}{k_p} \right) - \frac{\Delta k_p}{\Delta Q_p} k_s(\Omega) \\ q_{b,cy}(\Omega) &= -q_{0y}(-\Omega) = \pm q_{0y}(\Omega) \end{aligned} \quad (\text{A10})$$

where the last equality follows from the symmetry of equations (A9) and (A6) with respect to the exchange $\Omega \rightarrow -\Omega$.

The resonance.

We use here the resonance condition in Eq. (24) $\vec{q}_0(\Omega) + \vec{q}_0(-\Omega) = \vec{Q}_{1,2}$. This equation can be always satisfied for the y-coordinate, since $F_j(\Omega)$ in Eq.(A9) is an even function of Ω , so that one can choose $q_{0y}(-\Omega) = -q_{0y}(\Omega)$. For the x-coordinate, using Eq.(A7), it requires that

$$Q_1 + Q_2 + [k_s(\Omega + k_s(-\Omega))] \left(\frac{\Delta k_p}{\Delta Q_p} - \frac{Q_1 + Q_2}{2k_p} \right) = Q_{1,2} \quad (\text{A11})$$

$$\begin{aligned} \rightarrow \frac{\Delta k_p}{\Delta Q_p} &= \frac{\theta_{p1} + \theta_{p2}}{2} - \theta_{p2,p1} \frac{k_p}{k_s(\Omega + k_s(-\Omega))} \\ &= \pm \frac{\theta_{p1} - \theta_{p2}}{2} + \theta_{p2,p1} \frac{\mathcal{D}_0(\Omega) - G_z}{k_p + \mathcal{D}_0(\Omega) - G_z} \end{aligned} \quad (\text{A12})$$

where, as usual, we approximated $\theta_{pj} \simeq \frac{Q_j}{k_p}$, and we used the identity $k_p = k_s(\Omega) + k_s(-\Omega) - \mathcal{D}_0(\Omega) + G_z$. First of all, we notice that the second term at r.h.s. of Eq.(A12) is a very small correction, because $|G_z - \mathcal{D}_0(\Omega)| \ll k_p$. Thus, Eq.(A12) cannot be satisfied when $\Delta k_p = 0$ because it would require $|\theta_{p1} - \theta_{p2}| \ll |\theta_{p2,p1}|$ (in practice that the pump modes are collinear). Therefore, the resonance cannot take place in the PPLT configuration considered in Sec.II, and from now on we focus on the BBO case only, setting $G_z = 0$.

We notice that in principle the r.h.s. of Eq.(A12) depends on the frequency. The only exception is when one of the pumps is not tilted, e.g. $\theta_{p1} = 0$. Then, by requiring that shared modes are generated by the other one, i.e. that $q_{0x}(\Omega) + q_{0x}(-\Omega) = Q_2$, for $\frac{\Delta k_p}{\Delta Q_p} = \frac{\theta_{p2}}{2} = \frac{\theta_{p1} + \theta_{p2}}{2}$ the resonance takes place simultaneously at all the frequencies. However, even when this "magic" configuration is not considered, the bandwidth of modes that enter into resonance is so huge that can be practically considered infinite. We assume that Eq.(A12) is satisfied at degeneracy where $\mathcal{D}_0(0) = 0$, i.e. that

$$\frac{\Delta k_p}{\Delta Q_p} = \left(\frac{\Delta k_p}{\Delta Q_p} \right)_{res} = \pm \frac{\theta_{p1} - \theta_{p2}}{2} \quad (\text{A13})$$

Then, at a frequency $\Omega \neq 0$ the relative correction to the resonance condition in Eq.(A12) is on the order $\frac{\mathcal{D}_0(\Omega)}{k_p} \approx \frac{1}{k_p} k_s'' \Omega^2 = \frac{\Omega^2}{\Omega_B^2}$, where $\Omega_B = \sqrt{\frac{k_p}{k_s''}} \approx 2 \times 10^{16} \text{ s}^{-1}$. Thus, for any practical purpose, condition (A13) can be taken as *the* resonance condition.

A further insight into the problem is gained by approximating the incremental ratio in Eq. (A8) with its Taylor expansion. It turns out that the lowest order approximation is not precise enough, therefore we choose to expand each k_{pj} around the middle point $\bar{Q}_p = \frac{Q_1 + Q_2}{2}$ as $k_{p2,p1} = k_p(\bar{Q}_p) \pm \frac{dk_p}{dQ} \Big|_{\bar{Q}_p} \frac{\Delta Q_p}{2} + \frac{1}{8} \frac{d^2 k_p}{dQ^2} \Big|_{\bar{Q}_p} \Delta Q_p^2 + O(\Delta Q_p^3)$. In this way, $\frac{\Delta k_p}{\Delta Q_p} = \frac{dk_p}{dQ} \Big|_{\bar{Q}_p} + O(\Delta Q_p^2)$. Therefore, up to first order in ΔQ_p one has

$$\frac{\Delta k_p}{\Delta Q_p} \simeq \frac{dk_p}{dQ} \Big|_{\bar{Q}_p} = \frac{1}{k_p} \frac{dk_p}{d\theta_p} \Big|_{\bar{\theta}_p} = \frac{1}{k_p} \frac{dk_p}{d\gamma} \frac{d\gamma}{d\theta_p} \Big|_{\bar{\theta}_p} \quad (\text{A14})$$

where $\bar{\theta}_p = \frac{\theta_{p1} + \theta_{p2}}{2}$, and we remind that γ is the angle formed by the pump propagation direction with the optical axis. In this expression we recognize that the quantity $\frac{1}{k_p} \frac{dk_p}{d\gamma} = -\rho_\gamma$ is the *walk-off angle* formed by the wave-vector of the extraordinary wave and its Poynting vector, representing the direction of the energy flux. [33] It depends on the angle γ , but we make a small error in taking it at the cut angle γ_0 , $\rho_\gamma \rightarrow \rho_0 \simeq 0.0744 \text{ radians} = 4.26^\circ$. Thus, with a precision up to first order in the small quantities the following expression holds:

$$\frac{\Delta k_p}{\Delta Q_p} = -\rho_\gamma \frac{d\gamma}{d\theta_p} \Big|_{\bar{\theta}_p} \quad (\text{A15})$$

On the other side, the functional dependence of the angle γ on the tilt angle θ_p is provided by Eq.(A4). By differentiating this expression with respect to θ_p , one gets

$$\begin{aligned} \frac{d\gamma}{d\theta_p} &= -\sin \beta \cos \theta_p \frac{\sin \gamma_0}{\sin \gamma} + \sin \theta_p \frac{\cos \gamma_0}{\sin \gamma} \\ &\rightarrow \begin{cases} \mp 1 & \text{for } \beta = \pm \frac{\pi}{2} \\ -\sin \beta + \sin \theta_p \frac{1}{\tan \gamma_0} & \text{for } |\beta| \ll \frac{\pi}{2} \end{cases} \end{aligned} \quad (\text{A16})$$

The resonance condition of Eq. (A13) can then be reformulated in terms of the tilt angles of the two pumps as

$$\pm \frac{\theta_{p1} - \theta_{p2}}{2} = \rho_\gamma \left(\sin \beta \cos \theta_p \frac{\sin \gamma_0}{\sin \gamma} - \sin \theta_p \frac{\cos \gamma_0}{\sin \gamma} \right) \Big|_{\theta_p = \bar{\theta}_p} \quad (\text{A17})$$

$$\simeq \begin{cases} +\rho_{\bar{\gamma}} & \beta = +\frac{\pi}{2} \\ -\rho_{\bar{\gamma}} & \beta = -\frac{\pi}{2} \\ \rho_0 \left(\sin \beta - \frac{\theta_{p1} + \theta_{p2}}{2} \frac{1}{\text{tg } \gamma_0} \right) & |\beta| \ll \frac{\pi}{2} \end{cases} \quad (\text{A18})$$

This condition can be understood as a requirement on the pump tilt angles, for a fixed angle of rotation β of the crystal, or viceversa, for given pump tilts θ_{p1}, θ_{p2} as a receipt for the angle of rotation of the crystal at which resonance takes place.

$$\sin(\beta^{\text{res}}) = \pm \frac{\theta_{p1} - \theta_{p2}}{2\rho_0} + \frac{\theta_{p2} + \theta_{p1}}{2 \text{tg } \gamma_0} \quad (\text{A19})$$

-
- [1] S. Armstrong, M. Wang, R.Y. Teh, Q. Gong, Q. He, J. Janousek, H.-A. Bachor, M.D. Reid, and P.K. Lam, “Multipartite einstein-podolsky-rosen steering and genuine tripartite entanglement with optical networks,” *Nature Physics* **11**, 167–172 (2015).
- [2] Robert Raussendorf and Hans J. Briegel, “A one-way quantum computer,” *Phys. Rev. Lett.* **86**, 5188–5191 (2001).
- [3] Nicolas C. Menicucci, Peter van Loock, Mile Gu, Christian Weedbrook, Timothy C. Ralph, and Michael A. Nielsen, “Universal quantum computation with continuous-variable cluster states,” *Phys. Rev. Lett.* **97**, 110501 (2006).
- [4] Hans J. Briegel and Robert Raussendorf, “Persistent entanglement in arrays of interacting particles,” *Phys. Rev. Lett.* **86**, 910–913 (2001).
- [5] Jing Zhang and Samuel L. Braunstein, “Continuous-variable gaussian analog of cluster states,” *Phys. Rev. A* **73**, 032318 (2006).
- [6] Quntao Zhuang, Zheshen Zhang, and Jeffrey H. Shapiro, “Distributed quantum sensing using continuous-variable multipartite entanglement,” *Phys. Rev. A* **97**, 032329 (2018).
- [7] Peter van Loock, Christian Weedbrook, and Mile Gu, “Building gaussian cluster states by linear optics,” *Phys. Rev. A* **76**, 032321 (2007).
- [8] Mitsuyoshi Yukawa, Ryuji Ukai, Peter van Loock, and Akira Furusawa, “Experimental generation of four-mode continuous-variable cluster states,” *Phys. Rev. A* **78**, 012301 (2008).
- [9] S. Yokoyama, R. Ukai, S.C. Armstrong, C. Sornphiphatphong, T. Kaji, S. Suzuki, J.-I. Yoshikawa, H. Yonezawa, N.C. Menicucci, and A. Furusawa, “Ultra-large-scale continuous-variable cluster states multiplexed in the time domain,” *Nature Photonics* **7**, 982–986 (2013).
- [10] C. Navarrete-Benlloch, R. Garca-Patran, J.H. Shapiro, and N.J. Cerf, “Enhancing quantum entanglement by photon addition and subtraction,” *Physical Review A - Atomic, Molecular, and Optical Physics* **86** (2012), 10.1103/PhysRevA.86.012328.
- [11] H. Takahashi, J.S. Neergaard-Nielsen, M. Takeuchi, M. Takeoka, K. Hayasaka, A. Furusawa, and M. Sasaki, “Entanglement distillation from gaussian input states,” *Nature Photonics* **4**, 178–181 (2010).
- [12] D. Daems, F. Bernard, N. Cerf, and M. Kolobov, “Tripartite entanglement in parametric down-conversion with spatially-structured pump,” *Journal of the Optical Society of America B* **27** (2010), 10.1364/JOSAB.27.000447.
- [13] R. Menzel, A. Heuer, D. Puhlmann, K. Dechoum, M. Hillery, M.J.A. Spahn, and W.P. Schleich, “A two-photon double-slit experiment,” *Journal of Modern Optics* **60**, 86–94 (2013), <https://doi.org/10.1080/09500340.2012.746400>.
- [14] E. Brambilla and A. Gatti, “Efficient parametric generation in a nonlinear photonic crystal pumped by a dual beam,” *Opt. Express* **27**, 30233–30248 (2019).
- [15] Alessandra Gatti, “Engineering multipartite entanglement in nonlinear photonic crystals,” *Phys. Rev. A* **101**, 053841 (2020).
- [16] Hailong Wang, Claude Fabre, and Jietai Jing, “Single-step fabrication of scalable multimode quantum resources using four-wave mixing with a spatially structured pump,” *Phys. Rev. A* **95**, 051802 (2017).
- [17] Shengshuai Liu, Yanbo Lou, and Jietai Jing, “Experimental characterization of multiple quantum correlated beams in two-beam pumped cascaded four-wave mixing process,” *Opt. Express* **27**, 37999–38005 (2019).
- [18] Kai Zhang, Wei Wang, Shengshuai Liu, Xiaozhou Pan, Jinjian Du, Yanbo Lou, Sheng Yu, Shuchao Lv, Nicolas Treps, Claude Fabre, and Jietai Jing, “Reconfigurable hexapartite entanglement by spatially multiplexed four-wave mixing processes,” *Phys. Rev. Lett.* **124**, 090501 (2020).
- [19] Ottavia Jedrkiewicz, Erica Invernizzi, Enrico Brambilla, and Alessandra Gatti, “Hot-spots and gain enhancement in a doubly pumped parametric down-conversion process,” *Opt. Express* **28**, 36245–36259 (2020).
- [20] O. Jedrkiewicz, A. Gatti, E. Brambilla, M. Levenius, G. Tamauskas, and K. Gallo, “Golden ratio gain enhancement in coherently coupled parametric processes,” *Sci. Rep.* **8** (2018), 10.1038/s41598-018-30014-7.

- [21] A. Gatti, E. Brambilla, K. Gallo, and O. Jedrkiewicz, “Golden ratio entanglement in hexagonally poled nonlinear crystals,” *Physical Review A* **98** (2018), 10.1103/PhysRevA.98.053827.
- [22] A. Gatti, R. Zambrini, M. San Miguel, and L. A. Lugiato, “Multiphoton multimode polarization entanglement in parametric down-conversion,” *Phys. Rev. A* **68**, 053807 (2003).
- [23] E. Brambilla, O. Jedrkiewicz, L. A. Lugiato, and A. Gatti, “Disclosing the spatiotemporal structure of parametric down-conversion entanglement through frequency up-conversion,” *Phys. Rev. A* **85**, 063834 (2012).
- [24] A. Gatti, H. Wiedemann, L. A. Lugiato, I. Marzoli, Gian-Luca Oppo, and Stephen M. Barnett, “Langevin treatment of quantum fluctuations and optical patterns in optical parametric oscillators below threshold,” *Phys. Rev. A* **56**, 877–897 (1997).
- [25] V. Berger, “Nonlinear photonic crystals,” *Phys. Rev. Lett.* **81**, 4136–4139 (1998).
- [26] N. G. R. Broderick, G. W. Ross, H. L. Offerhaus, D. J. Richardson, and D. C. Hanna, “Hexagonally poled lithium niobate: A two-dimensional nonlinear photonic crystal,” *Phys. Rev. Lett.* **84**, 4345–4348 (2000).
- [27] Ady Arie, Nili Habshoosh, and Alon Bahabad, “Quasi phase matching in two-dimensional nonlinear photonic crystals,” *Opt. Quant. Electron.* **39**, 361–375 (2007).
- [28] I. Dolev, A. Ganany-Padowicz, O. Gayer, A. Arie, J. Mangin, and G. Gadret, “Linear and nonlinear optical properties of mgo:litao3,” *Applied Physics B* **96**, 423–432 (2009).
- [29] C. C. Gerry and P. L. Knight, *Introductory Quantum Optics* (Cambridge University Press, 2005) Chap. 7, pp. 167–169, 182–187.
- [30] Alessandra Gatti, “Analysis of multipartite entanglement generated by doubly pumped parametric down-conversion processes,” (2020), unpublished.
- [31] Martin Levenius, Valdas Pasiskevicius, and Katia Gallo, “Angular degrees of freedom in twin-beam parametric down-conversion,” *Appl. Phys. Lett.* **101**, 121114– (2012).
- [32] L. Chen, P. Xu, Y. F. Bai, X. W. Luo, M. L. Zhong, M. Dai, M. H. Lu, and S. N. Zhu, “Concurrent optical parametric down-conversion in $\chi(2)$ nonlinear photonic crystals,” *Opt. Express* **22**, 13164–13169 (2014).
- [33] Max Born, Emil Wolf, A. B. Bhatia, P. C. Clemmow, D. Gabor, A. R. Stokes, A. M. Taylor, P. A. Wayman, and W. L. Wilcock, “Optics of crystals,” in *Principles of Optics: Electromagnetic Theory of Propagation, Interference and Diffraction of Light* (Cambridge University Press, 1999) p. 790–852, 7th ed.
- [34] N. Boeuf, David A. Branning, I. Chaperot, E. Dauler, S. Guerin, Gregg S. Jaeger, Antoine Muller, and Alan L. Migdall, “Calculating characteristics of noncollinear phase matching in uniaxial and biaxial crystals,” *Optical Engineering* **39**, 1016 – 1024 (2000).
- [35] K. Kato, “Second-harmonic generation to 2048 Å.. in $\hat{\Gamma}^1$ -ba2o4,” *IEEE Journal of Quantum Electronics* **22**, 1013–1014 (1986).
- [36] Samuel L. Braunstein, “Squeezing as an irreducible resource,” *Phys. Rev. A* **71**, 055801 (2005).
- [37] R. Simon, “Peres-horodecki separability criterion for continuous variable systems,” *Phys. Rev. Lett.* **84**, 2726–2729 (2000).
- [38] Peter van Loock and Akira Furusawa, “Detecting genuine multipartite continuous-variable entanglement,” *Phys. Rev. A* **67**, 052315 (2003).